

Thermal Overload Capabilities of an Electric Motor and Inverter Unit Through Modeling Validated by Testing

by

Henning Lohse-Busch

Thesis submitted to the faculty of the
Virginia Polytechnic Institute and State University
in partial fulfillment of the requirements for the degree of

MASTER OF SCIENCE
in
Mechanical Engineering

Committee,
Dr. Douglas J. Nelson, chair
Dr. Charles F. Reinholtz, member
Dr. Michael W. Ellis, member

May 28, 2004
Blacksburg, VA

Keywords: Integrated AC induction motor-inverter unit; Finite difference thermal model; Thermal overload; Automotive fuel cell air compressor motor

Thermal Overload Capabilities of an Electric Motor and Inverter Unit Through Modeling Validated by Testing

Henning Lohse-Busch

Abstract

VPT, Inc and the U.S. Dept. of Energy have sponsored the development of a high-speed 12 kW AC induction motor to drive automotive fuel cell air compressors. Thermal considerations and the cooling system are detailed in this paper As one part of the development.

The motor and inverter are packaged in one unit with the heat sink in the middle. The heat sink is a cold chamber designed to absorb the maximum heat losses from the unit. Empirical data was used to validate the model of the cold chamber and finalize the design.

A lumped capacitance finite-difference model was developed to simulate the entire motor inverter assembly. The individual components of the thermal model were tested and the data was used to calibrate and validate the thermal model.

Using the model, the thermal overload conditions were investigated. The limiting factors are the stator copper winding temperatures, which can damage the plastic slot liners. The double current test was simulated and operating temperatures of the system remained within thermal limits for 4 minutes.

As a conclusion from the model, the thermal resistances from the stator to the case or the heat sink need to be reduced. Integrating the motor casing and end plate to the heat sink, rather than building it in sections, would reduce the thermal contact resistances. Also the copper winding ends in the stator could be coated in material that would bond to the case, thus increasing heat transfer from the windings to the case.

Acknowledgements

I would like to thank the U.S. Department of Energy and VPT, Inc. for sponsoring the research, Dr. Konrad for his guidance as a project leader, my committee members for their support and Dr. Nelson for his support, guidance and help.

Table of contents

1	Introduction.....	1
1.1	Drive for fuel cell vehicles.....	1
1.2	Functioning and complexity of fuel cell systems	1
1.3	Pressurized fuel cell systems versus open air systems.....	2
1.4	Need for a compact motor-inverter unit.....	3
1.5	The thermal limitations.....	4
1.6	Mapping of the thesis.....	4
2	Literature review.....	5
3	Limiting factors in electric motor assemblies.....	6
3.1	Brief explanation of AC induction motors.....	6
3.1.1	AC induction motor	6
3.1.2	DC/AC inverter.....	6
3.1.3	AC induction motor advantages.....	7
3.2	Thermal limiting factors in AC induction motors and inverters.....	7
3.2.1	The copper windings in the motor	7
3.2.2	The IGBT in the inverter.....	7
3.2.3	Summary of limiting factors.....	8
3.3	Different conditions causing thermal limits.....	8
3.3.1	Steady state limits	8
3.3.2	Transient limits	9
4	Heat sink design.....	10
4.1	Motor-inverter unit design goals.....	10
4.2	Design requirements for the heat sink	10
4.3	Initial heat sink design ideas.....	11
4.4	Initial calculations.....	12
4.5	Cold chamber heat sink.....	13
4.6	Cold chamber testing	14
4.6.1	Test design	14
4.6.2	Test setup	15
4.6.3	Heat sink power resistor testing results	18
4.7	Cold chamber calculations.....	19
4.7.1	Mathematical model.....	19
4.7.2	Computer model.....	20
4.7.3	Design insights and decisions based on modeling.....	20
4.7.4	Testing data compared to model.....	22
4.8	Final design.....	22
5	The thermal model of the motor inverter assembly	24
5.1	The motor and inverter assembly.....	24
5.2	Lumped capacitance model and validity.....	25
5.3	Explicit finite difference method	25
5.4	The thermal resistance network	26
5.5	Dimensions for the modeling.....	27
5.6	Computation of the thermal resistances.....	27

5.7	The thermal model computational flow	28
5.7.1	Overview	28
5.7.2	Setup for the code	29
5.7.3	Explicit finite difference structure	30
5.7.4	Outputs	30
6	Inverter testing with power electronics	31
6.1	Test set up	31
6.1.1	Instrumentation plan and implementation	31
6.1.2	CPES test facility	32
6.1.3	Test procedures	33
6.2	Experimental Results	33
6.3	Comparison to the model	34
6.4	Conclusion and model adjustments	35
7	Motor Inverter Assembly	36
7.1	Test Setup	36
7.1.1	Instrumentation of the unit	36
7.1.2	Test Stand with Air Compressor	37
7.2	Experimental results	39
7.3	Comparison to model	40
7.4	Conclusion and model adjustments	41
8	Validation and review of the model	42
8.1	Steady state	42
8.2	Transients	42
9	Transient limitation of the unit and overload capabilities	43
9.1	Physical limiting factors	43
9.2	Maximum power condition	43
9.3	Double current condition	44
10	System strategies to improve the thermal limits	45
10.1	Active flow control	45
10.2	Capacity of the thermal reservoir	45
11	Conclusion	47
	References	48
	Appendix 1: Symbol reference guide	49
	Appendix 2: Convection heat transfer details	50
	Appendix 3: All the thermal resistances defined	54
	Appendix 4: The code to the thermal model	57
	Vita	70

Table of figures

Figure 1: Automotive type fuel cell system.....	1
Figure 2: Opcon twin-screw compressor and parts.....	2
Figure 3: Air compression system for automotive fuel cell system.....	3
Figure 4: Motor-inverter unit coupled to the air compressor.....	4
Figure 5: Sine wave approximation by inverter.....	6
Figure 6: Motor-inverter unit design in CAD view	10
Figure 7: Standard cold plate design.....	11
Figure 8: Heat dissipation as a function of flow rates and pipe length.....	12
Figure 9: Chamber heat sink design.....	13
Figure 10: Heat sink test setup design with power resistors.....	15
Figure 11: Heat sink with adjustable guides and the power resistors for testing.....	16
Figure 12: Entire test setup for heat sink with power resistor	17
Figure 13: Results from heat sink testing with power resistors.....	18
Figure 14: Mathematical cold chamber approximation.....	19
Figure 15: Half inch cold chamber thickness case study results (based on a 20 deg C temperature differential)	20
Figure 16: Cold chamber heat dissipation as a function of chamber thickness and coolant flow rates (based on a 20 deg C temperature differential).....	21
Figure 17: Heat sink test data compared to the model.....	22
Figure 18: Final heat sink design.....	23
Figure 19: Thermal mass composing the inverter-motor unit	24
Figure 20: Thermal network for the motor inverter unit.....	26
Figure 21: Dimension of the assembly for the model.....	27
Figure 22: Flow of the thermal model computation	28
Figure 23: Finite difference code structure.....	30
Figure 24: Schematic showing the thermocouple placements on the inverter.....	31
Figure 25: Instrumentation of the heat sink and inverter.....	32
Figure 26: CPES testing facility	33
Figure 27: Inverter testing results at CPES.....	34
Figure 28: Temperatures computed by the model for the CPES test.....	35
Figure 29: Motor inverter instrumentation plan.....	36
Figure 30: Motor instrumentation.....	37
Figure 31: Air compressor testing setup	38
Figure 32: Air compressor motor coupling and coolant system.....	39
Figure 33: Complete motor inverter unit test results (10000 rpm & 10 psi)	40
Figure 34: Full test model results with empirical data.....	41
Figure 35: Maximum continuous power run simulation.....	43
Figure 36: Double current simulation.....	44
Figure 37: Flow influence over the system.....	45
Figure 38: Thermal capacity influence on the system	46

Table of tables

Table 1: IGBT characteristics from Semikron specification sheet	8
Table 2: Major thermal limiting factor of the inverter and motor	8
Table 3: List of the thermal masses and their specification.....	25
Table 4: Losses in the different motor and inverter constituents.....	29
Table 5: Major thermal limiting factor of the inverter and motor	43

1 Introduction

1.1 Drive for fuel cell vehicles

In the last 5 years, fuel cell powered vehicles attract more and more attention. The zero emission capability of a fuel cell system, the renewable hydrogen fuel and the high efficiency are the advantages that the automotive industry praises. The fuel cell stack produces electricity and water through direct chemical conversion of hydrogen and oxygen. This electric power allows electric motors to spin the wheels and drive a vehicle down the road.

1.2 Functioning and complexity of fuel cell systems

An automotive type fuel cell stack needs supporting systems, such as a thermal management system, a fuel delivery system and an air supply and conditioning system. The thermal system maintains the operating temperature of the fuel cell at optimal levels. The fuel delivery system provides the fuel cell stack with enough hydrogen at the right pressure, temperature and humidity. The air supply and conditioning system supplies the fuel cell with enough air at the right pressure, temperature and humidity. All these system quickly translate into complex arrangements in a real vehicle. Figure 1 shows a simple automotive fuel cell stack with its supporting system.

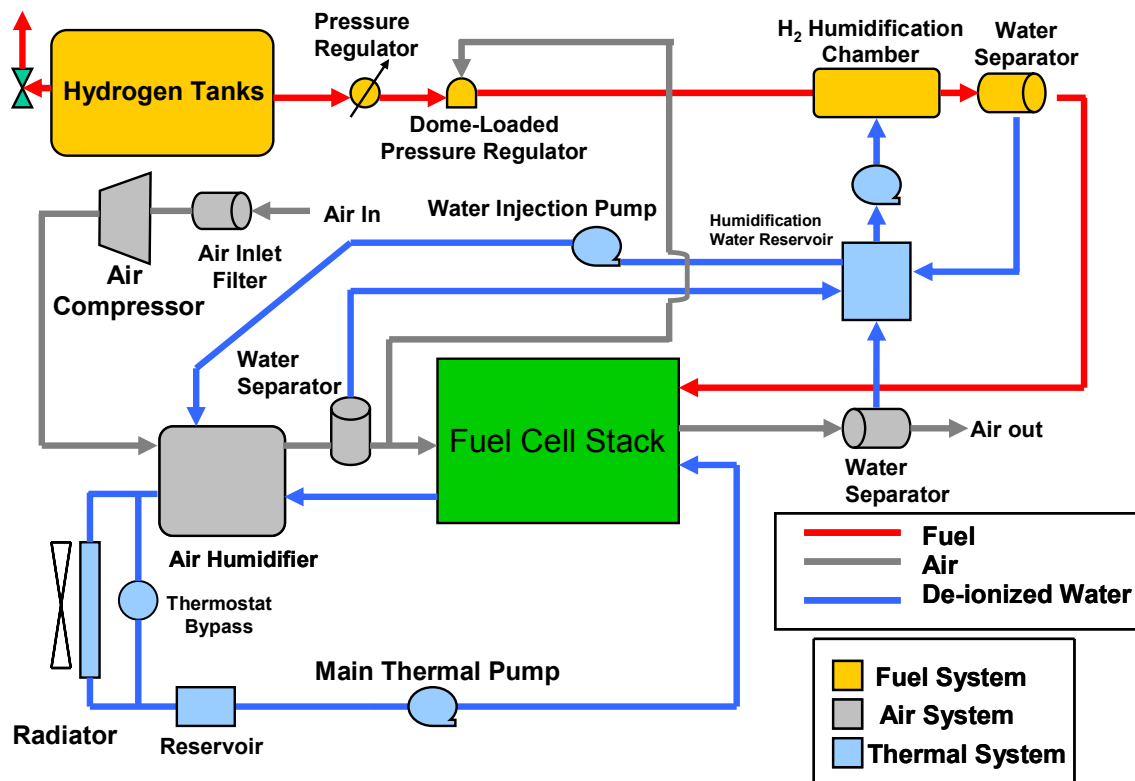


Figure 1: Automotive type fuel cell system

1.3 Pressurized fuel cell systems versus open air systems

To provide more specific power and increase efficiency, automotive fuel cell systems are pressurized. The air supply is pressurized before being conditioned and fed into the fuel cell stack. This requires a compressor to boost the air pressure. In an 80 kW system, as much as 10 kW can be used to compress air to improve the power output and the efficiency of the fuel cell stack. About 10% of the total electric output of a fuel cell stack goes to the compressor (*Larminie, 2000*).

Twin screw compressors are widely used for automotive fuel cell applications due to the compact and light package and the ability to maintain a given pressure ratio over wide ranges of air mass flow rates. Galen Kulp's work (*Kulp, 2001*) indicates the higher effectiveness of twin screw compressors in a variety of domains from efficiency to water management and temperature conditions. Figure 2 shows an Opcon twin screw compressor used by Virginia Tech in their automotive fuel cell system. Ford and Daimler-Chrysler use the same compressor in their fuel cell vehicles such as the fuel cell Ford Focus and the NECAR 5. These compressors run at rotational speeds of 12,000 rpm to 15,000 rpm.

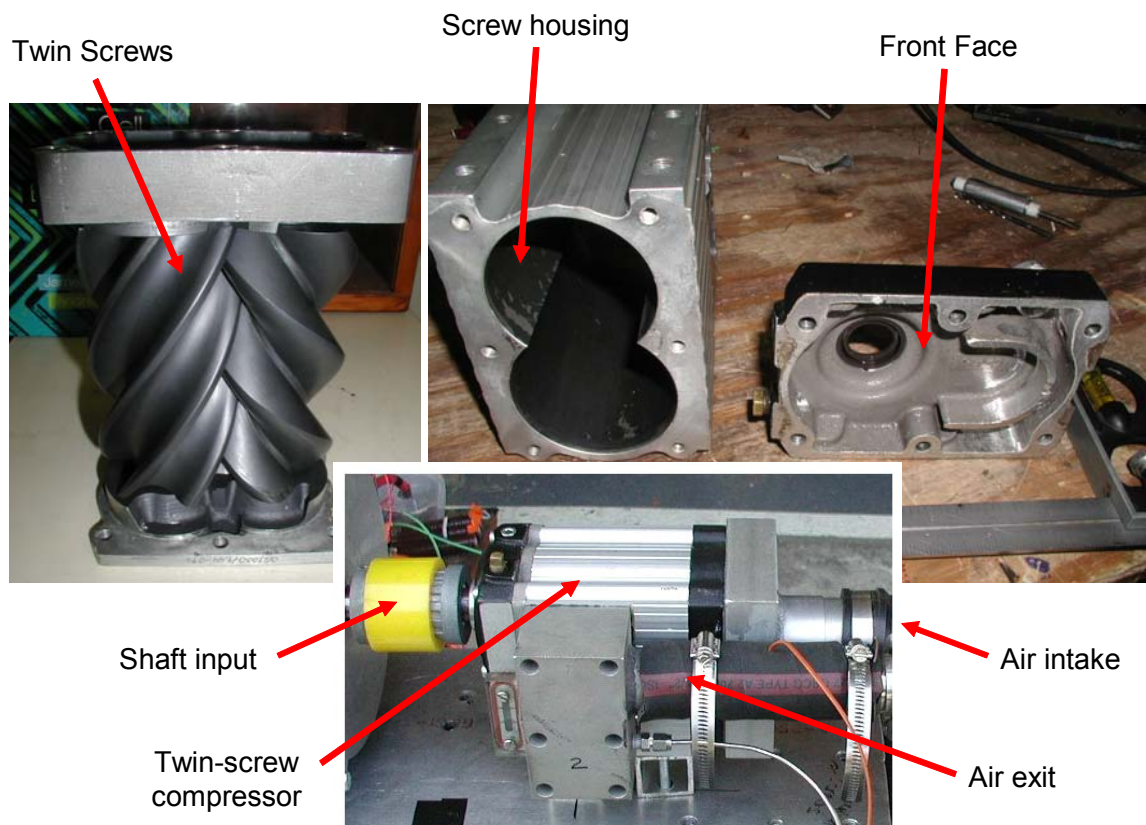


Figure 2: Opcon twin-screw compressor and parts

1.4 Need for a compact motor-inverter unit

Electric motors are required to drive these compressors since there is no rotating part in a fuel cell stack as there would be in an engine. AC induction motors in the 10 to 12 kW range with high speed required by the compressors are rare. Moreover, these motors require a separate inverter to drive the motor from the high voltage DC power source on-board the vehicle. AC induction motors can be designed to be as efficient as the other electric motor architectures. The efficiency of the motor will impact the overall system efficiency. Since high efficiency is the key in automotive fuel cell systems, the efficiency of the motor driving the air compressor is important.

One of the greatest challenges of fuel cell vehicles is the packaging of all the systems. Figure 3 is a picture of the air compression system used in Virginia Tech's fuel cell hybrid in 2001. The electric motor is in a large industrial casing. The motor requires a large variable speed drive, which in turn requires DC input voltage and converts it into AC power with the right frequency. Both these component are large, bulky and rather heavy. The long power cables are a source of electromagnetic fields which can interfere with the electronics in a vehicle.

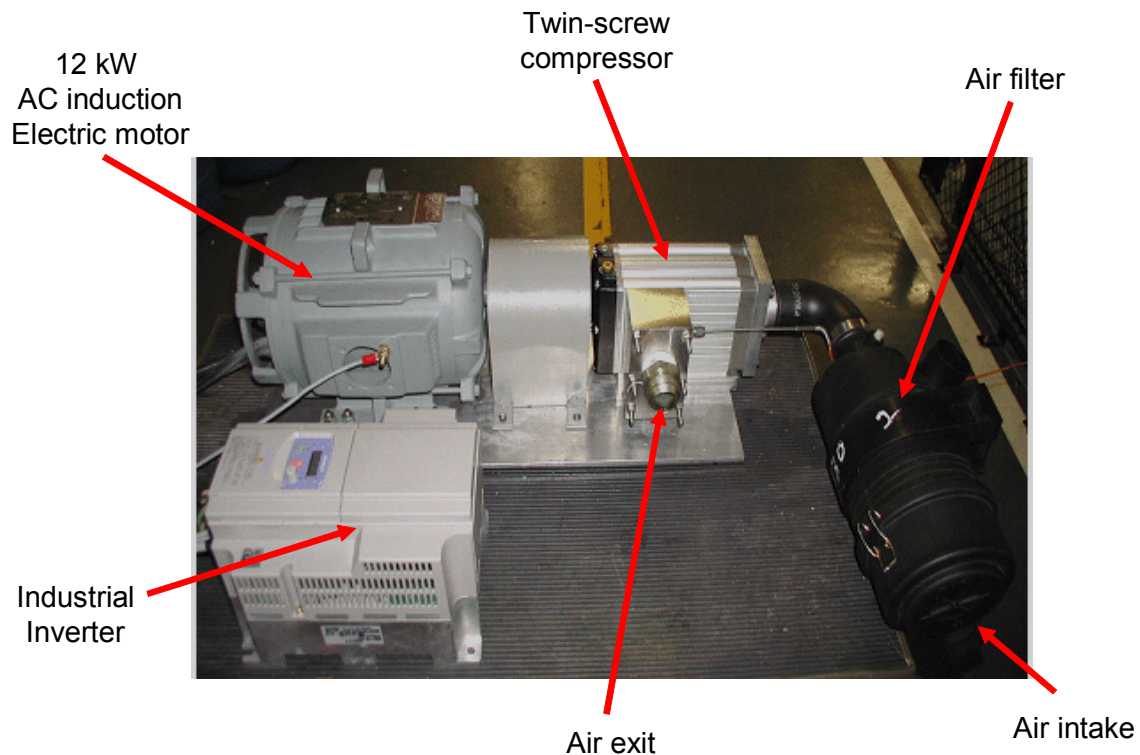


Figure 3: Air compression system for automotive fuel cell system

In partnership with Virginia Power Technologies and DOE, a small group at Virginia Tech designed and developed a compact and light high-speed 12 kW AC induction inverter-motor assembly to address these issues. The motor and inverter are assembled in one unit with an aluminum housing. The entire assembly is contained in one aluminum cylinder 8 inches in diameter and 12 inches long.

The power electronics of the inverter was designed by Christopher Smith and the motor was designed by Dr. Konrad. Figure 4 illustrates the end product. Compared to the system shown in Figure 3, the integrated system is much more compact.



Figure 4: Motor-inverter unit coupled to the air compressor

1.5 The thermal limitations

The integration of the inverter and the motor into one unit creates several challenges to overcome. Besides the design and packaging, a large concern is the temperature limits of the components. The motor and the inverter temperatures increase during operation and the temperatures of components will become the limiting factor to continuous high power operation. The thermal limiting factors in steady state conditions and transient conditions are the center of this study.

1.6 Mapping of the thesis

This document starts by defining the specifications on the thermal limits, followed by the initial design approach of the inverter-motor unit cooling. The thermal model is developed to simulate different extreme conditions. Next, the testing of the individual parts and the full unit are presented. A comparison between the model and real test data serves to calibrate and validate the simulations. Finally, thermal limiting cases are simulated to analyze the overload capabilities of the unit and possible system cooling strategies are investigated.

2 Literature review

The Visteon Corporation performed a thermal analysis (*Turnbull, 2003*) of a 25 kW permanent magnet motor. The motor is applied in the drive line between the engine and the transmission, which is a harsher environment than a fuel cell compressor would experience. The major losses in the motor were the copper losses in the windings, the stator iron losses due to the rotational magnetic flux, the rotor iron losses and the mechanical losses. The study used energy conservation in combination with commercial finite element software. Measured data was used to tune the model parameters. The liquid cooled system was modeled and experimental data results are used to calibrate the model to improve accuracy.

3 Limiting factors in electric motor assemblies

3.1 Brief explanation of AC induction motors

3.1.1 AC induction motor

An AC induction motor is composed of a rotor and a stator. The rotor is composed of aluminum and steel. The rotor responds to magnetic fields. The magnetic fields that drive the rotor are created in the stator copper windings. By circulating an AC current through these windings fluctuating magnetic fields are created. The rotor tries to follow these fields causing it to spin. The rotor spins with some slip, which means that the stator fields are faster than the speed of the rotor, which creates torque.

3.1.2 DC/AC inverter

The inverter synthesizes an AC waveform from a DC energy source. Inverters are digitally controlled and the sine waves are approximations. The voltage is changed from zero to a maximum during a given fraction of a period, but the current in the windings can not change instantaneously, therefore the voltage can only reach an average value in a given period. The voltage is changed by a special fast high-power switching device called an IGBT (insulated gate bipolar transistor). The width of the on-time of the switch is called the duty cycle. The larger the duty cycle, the higher the voltage. Figure 5 illustrates a sine wave generator using pulse width modulation. The period is always constant but the width of the pulse changes. The longer the width of the pulses the higher the average voltage.

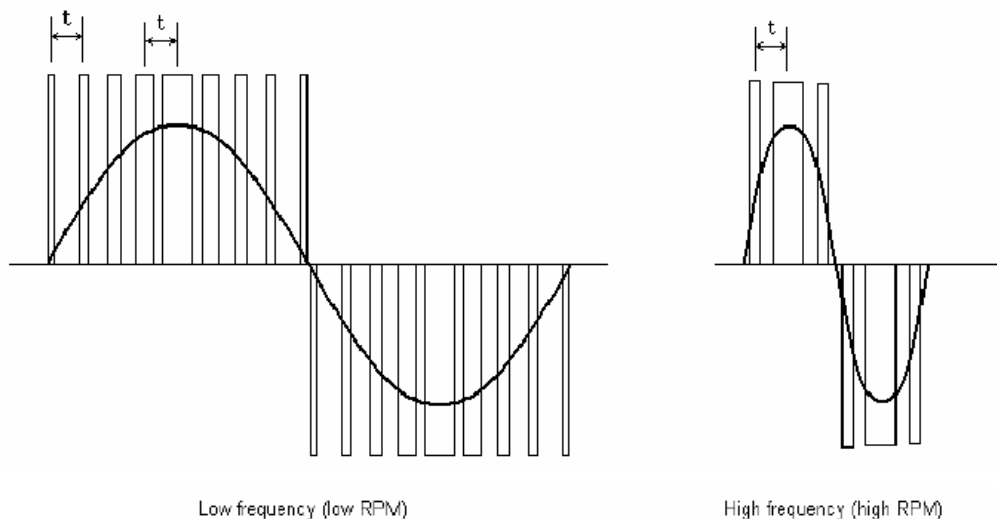


Figure 5: Sine wave approximation by inverter

Higher voltage amplitude on the sine wave creates higher current in the windings which generates larger torques on the rotor.

3.1.3 AC induction motor advantages

AC induction motors are advantageous for high speeds and high efficiencies. The high speeds are required by the twin screw compressor. The high speed also implies high power in smaller package and direct coupling to the compressor (no gearbox).

3.2 Thermal limiting factors in AC induction motors and inverters

3.2.1 The copper windings in the motor

The current in the windings creates ohmic losses which directly translate into internal heating of the copper in the windings. The heating of the copper is calculated using the current and the wire resistance as shown in Equation 1.

$$P_{heat} = I^2 \cdot R_{wire} \quad \text{Equation 1}$$

High temperature in the copper windings will melt the plastic insulated slot liners used in the structure of the stator and eventually even melt the insulation of the copper itself. Therefore the temperature of the copper windings represents the first limiting thermal factor.

All the losses are defined in section 5.7.2.

3.2.2 The IGBT in the inverter

The IGBT switches in the inverter that synthesize the AC sin waves for the stator are high power devices which switch extremely fast. The design uses a Semikron Semitrans® Six-pack Superfast IGBT Modules SKM 100 GD 063 DL (*Siemens, 2004*). The IGBT's have switching and conduction losses which cause them to heat up. High temperatures can which can cause a drop in the power processing capabilities or worse the destruction of the device itself. Therefore the temperature of the IGBT's is a thermal limiting factor.

Table 1 presents the characteristics of the IGBT used in the design.

Table 1: IGBT characteristics from Semikron specification sheet

Absolute Maximum Ratings		Values			Units
Symbol	Conditions ¹⁾				
V _{CEs}				600	V
V _{CGR}	R _{GE} = 20 kΩ			600	V
I _C	T _{case} = 25/70 °C			130 / 100	A
I _{CM}	T _{case} = 25/70 °C; t _p = 1 ms			150 / 150	A
V _{GES}				± 20	V
P _{tot}	per IGBT, T _{case} = 25 °C			450	W
T _j , T _{stg}				-40 ... +150 (125)	°C
V _{isol}	AC, 1 min.			2500	V
humidity	DIN 40040			Class F	
climate	DIN IEC 68 T.1			40/125/56	

Characteristics					Units
Symbol	Conditions ¹⁾	min.	typ.	max.	
Thermal characteristics					
R _{thjc}	per IGBT	-	-	0,27	°C/W
R _{thjc}	per diode	-	-	0,6	°C/W
R _{thch}	per module	-	-	0,05	°C/W

3.2.3 Summary of limiting factors

Table 2 summarizes the major thermal limiting factors in the motor and inverter.

Table 2: Major thermal limiting factor of the inverter and motor

	Limiting temperature	Comment
IGBT junction	125 deg C	Exceeding temperature results in power loss or damage to the device
Copper Stator windings	160 deg C	Exceeding temperature results in damage to the plastic slot liners

3.3 Different conditions causing thermal limits

3.3.1 Steady state limits

The motor-inverter unit needs to operate at the 10 kW power levels for long times without running into thermal limits. In other words, the steady state temperatures of the different components need to stay below the limiting temperatures.

For steady state operating conditions, the design needs to operate without overheating while the coolant system is operational. It is important that all components in the motor or the inverter have sufficient thermal paths to transfer the heat toward the heat sink. The heat sink must be designed to remove all the heat generated in the different parts of the assembly.

The worst case steady state condition is at maximum power and maximum ambient temperatures. This can be defined by a power production of 10 kW at 12,000 rpm with an ambient temperature of 60 deg C.

3.3.2 Transient limits

The motor-inverter unit is capable of producing higher peak power for a limited amount of time. But at high power, components suffer greater losses and heat generation, which rapidly pushes the temperatures to their limits. Electric motors have a continuous power rating (steady state) and a peak power rating, which is limited in time due to thermal limits. Peak temperatures are reached in these transient phases.

The interest is on the double current case and the time of operation before the components reach temperature limits. The motor requires more power to reach the maximum operation temperature; this is known as the double current condition. The inverter is designed to be able to supply double the steady state current rating for accelerating the motor/compressor and for peak power conditions.

4 Heat sink design

4.1 Motor-inverter unit design goals

The base goals for the entire motor inverter unit are to fit the entire assembly in a cylinder 8 inches in diameter and a length of 12 inches. The motor fits naturally into the cylinder shape and the inverter is specially designed to fit a short barrel. This requires the heat sink to be a cylinder 8 inches in diameter. Figure 6 shows the heat sink sandwiched between the motor and the inverter.

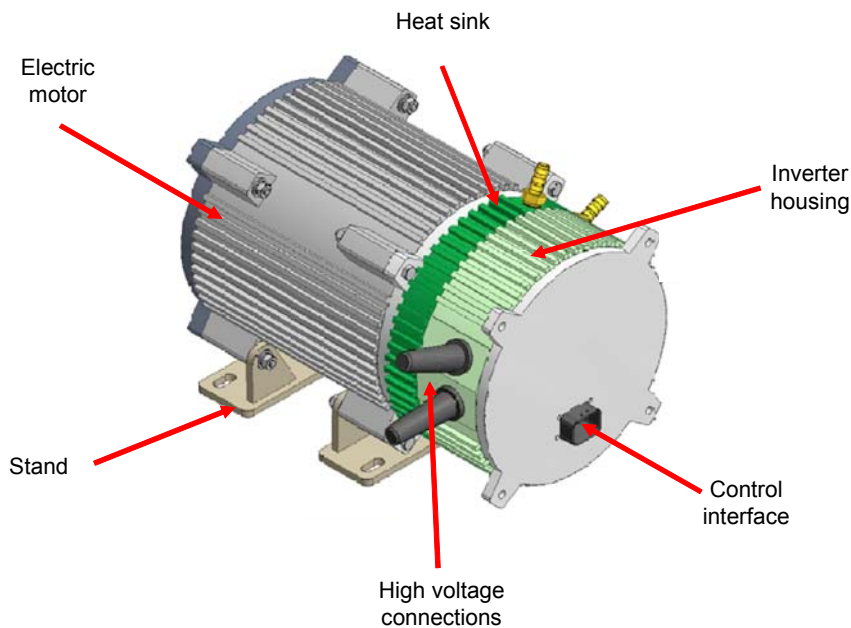


Figure 6: Motor-inverter unit design in CAD view

4.2 Design requirements for the heat sink

The heat sink must absorb enough energy to keep the motor-inverter unit parts cool enough to prevent power loss or damage. At full power and maximum speed the losses from the motor and the inverter total 866 W. With a factor of safety to over design rather than under design, the goal is to design a heat sink to dissipate 1000 W.

Due to the packaging constraints, air cooling does not appear feasible. The heat sink fins would have to be large and heavy. The sandwich architecture and round barrel approach do not allow for easy fan integration. Finally, forced air convection does not allow sufficient heat transfer rate with the low temperature differences and small area involved in this design.

A water cooled approach is much more effective and compact. With the heat sink in between the motor and the inverter, it needs to remove heat from both the motor and

inverter. The water cooled heat sink effectively cools both sides. Most electronics coolant loops for electric or hybrid vehicles are designed for 3 gpm (0.19 kg/s) flow rates. For example a Ford EV Ranger had an electronics coolant loop that requires 3 gpm. The same cooling requirements apply to a 67 kW peak Siemens inverter (*Siemens, 2004*) are used to drive a large AC induction motor for after market electric vehicle conversions.

Finally some other factors affect the heat sink design. These factors are not related to the thermal limits. The three phase cables need to go from the inverter through the heat sink to the windings in the motor. The heat sink should also provide shielding from the electro-magnetic fields generated by the current flowing through the windings in the stator. This heat sink should also be easy to manufacture.

4.3 Initial heat sink design ideas

After a careful analysis of existing heat sinks, a cold plate arose as an interesting design. Figure 7 illustrates a cold plate integrated into the packaging scheme. Standard cold plates are designed to have two or more passes of a pipe through a material with a high thermal conductivity. The coolant circulation in the pipe absorbs energy through convection heat transfer between the liquid and the pipe wall. The material with high thermal conductivity increases the energy transfer on the underlying areas increasing the heat transfer to the coolant in the pipe. The pipe diameter comes in different sizes depending on the application. Cold plates such as the one shown in Figure 7 are commercially available at several companies.

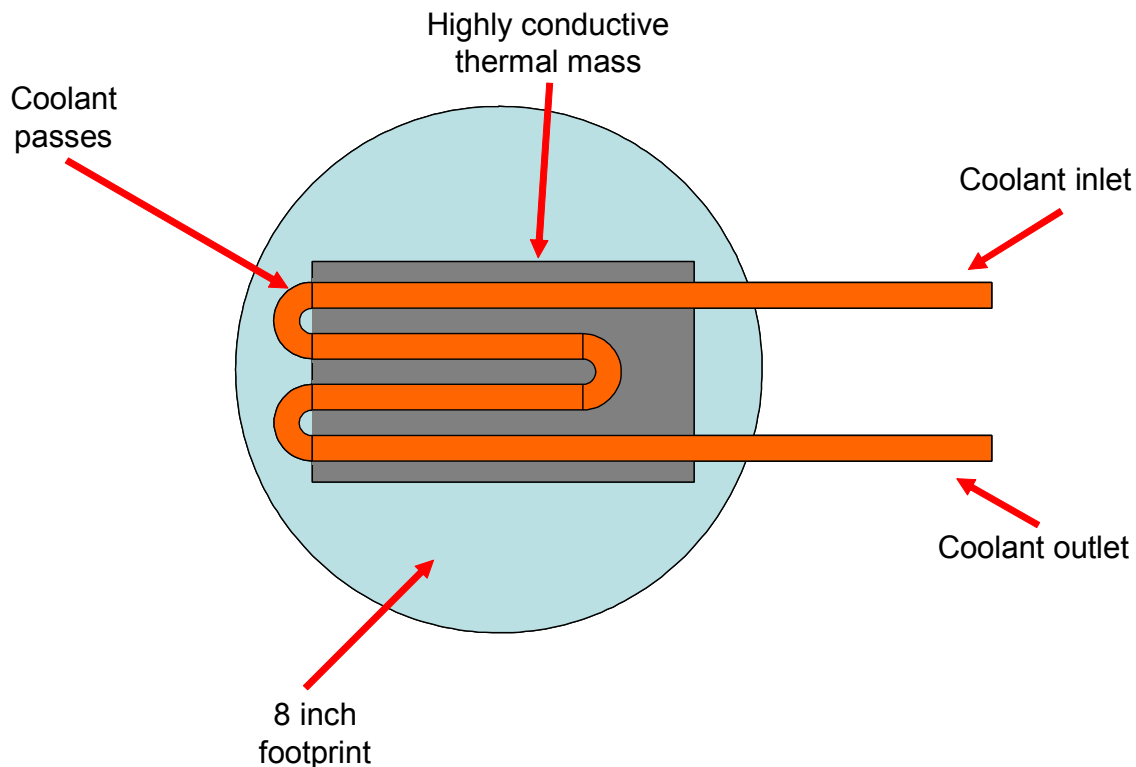


Figure 7: Standard cold plate design

4.4 Initial calculations

At the start, the simple heat absorption of coolant in a simple pipe was considered. A simple model based on convection heat transfer with constant surface temperature was used. Equation 2 is the base equation used for this initial application.

$$q_{conv} = hA_s \Delta T_{lm} \quad \text{Equation 2}$$

The detailed calculations applied to a pipe are given in Appendix 2.

Figure 8 presents the results of this initial approach. The ceiling represents the 1000 W heat absorption to the coolant. As expected the increased pipe length allows for increased heat transfer since the surface area increases. A higher flow rate increases the heat transfer since more mass in a given period is available to absorb the heat and the convection coefficient increases. At the 3 gpm flow rate a pipe length of 8 inches is required to absorb 1000 W. A 16 inch pipe length represent a double pass of a pipe in the unit, and at the 3 gpm flow rate the heat transfer would be above 1700 W which is well above the ceiling.

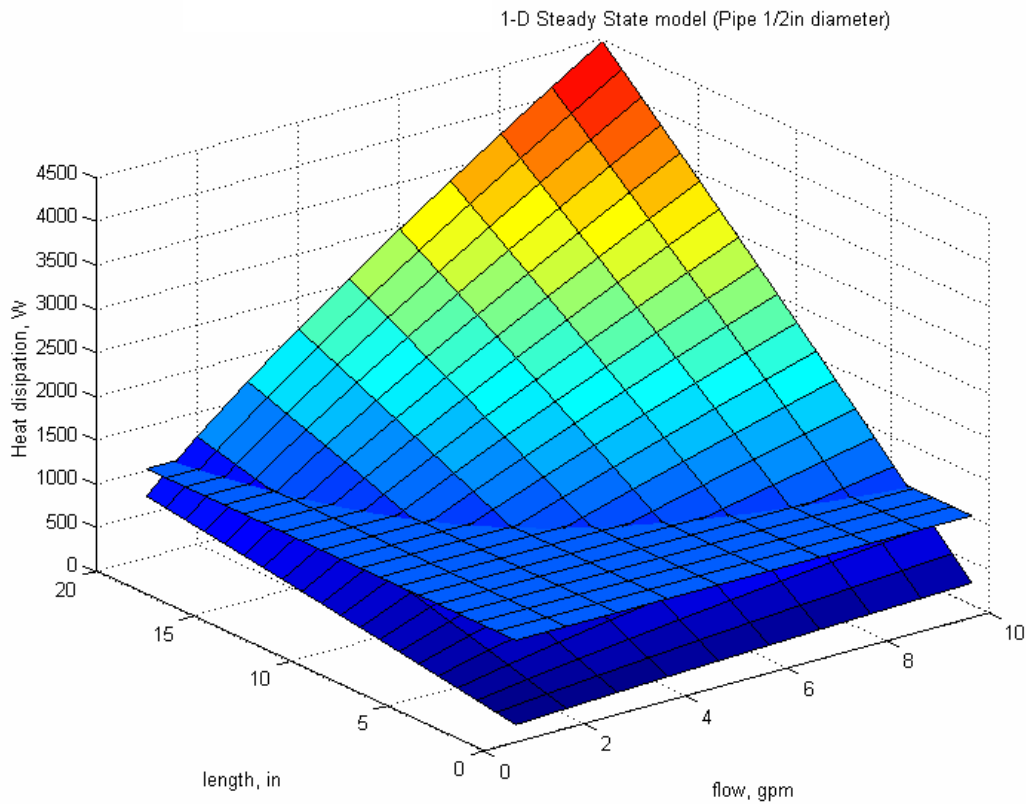


Figure 8: Heat dissipation as a function of flow rates and pipe length

As a conclusion, the pipe model confirms that a 3 gpm flow rate can transfer heat at a rate of 1000 W required to cool inverter-motor unit. But the integration of industrial cold plates in the cylindrical motor-inverter unit presents some disadvantages. The first is the physical integration of a square cold plate in the round design while maintaining low thermal resistance paths to the motor and the inverter. The second major disadvantage is the cost of a prepackaged unit. For production of the motor inverter unit, the supplier of the cold plate could have considerable impact on the manufacturing price.

4.5 Cold chamber heat sink

The cold chamber is a cylinder 8 inches in diameter and small thickness (1/4 to 2 inches). The performance of cold chamber can be increased by placing appropriate guides inside the chamber itself to restrict the flow to desired areas, which increases the coolant flow velocity. Figure 9 illustrates the cold chamber concept.

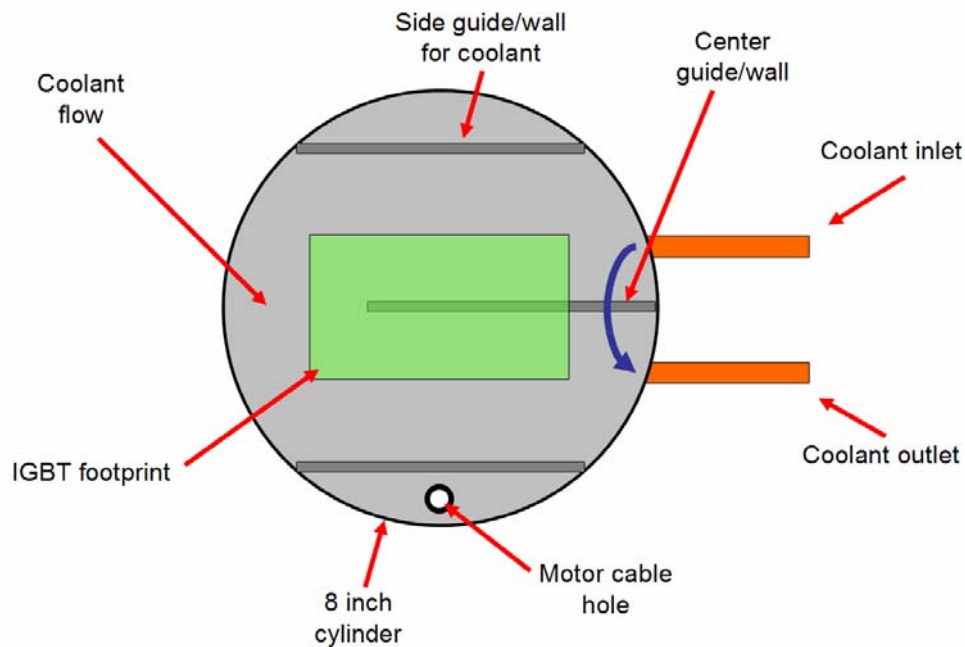


Figure 9: Chamber heat sink design

The IGBT is directly mounted on the heat sink. The center wall forces the coolant to flow all the way around the chamber. The side wall restricts the flow in such a way that IGBT gets maximum coolant flow under it. This design also allows implementing the through hole for the 3 phase cables from the inverter to the motor.

The location of the side guides is a significant part of the testing. The thermal model contains an approximation of this cold chamber and testing of the heat sink with variable side guides was used to verify the model.

4.6 Cold chamber testing

4.6.1 Test design

In order to design the cold chamber guide, a heat sink chamber was machined to take some test data. This data is used to validate the modeling of the cold chamber addressed in section 4.7. Different guide positions were tested to determine the best arrangement.

Since running the IGBT requires gating circuitry and a load bank, power resistors are used to simulate the IGBT heating. Four power resistors can be arranged in such a way that they cover the footprint of the IGBT. Using electric power through these resistors results in direct heat dissipation in the resistors. Equation 3, which is Ohm law ($V = RI$) combined with the power equation ($P = VI$), shows how to compute the dissipated power in the resistors. R is the equivalent resistance of the four resistors combined.

$$P_{dissipated} = RI^2 \quad \text{Equation 3}$$

Figure 10 illustrates the heat sink test setup with the power resistors instead of the IGBT.

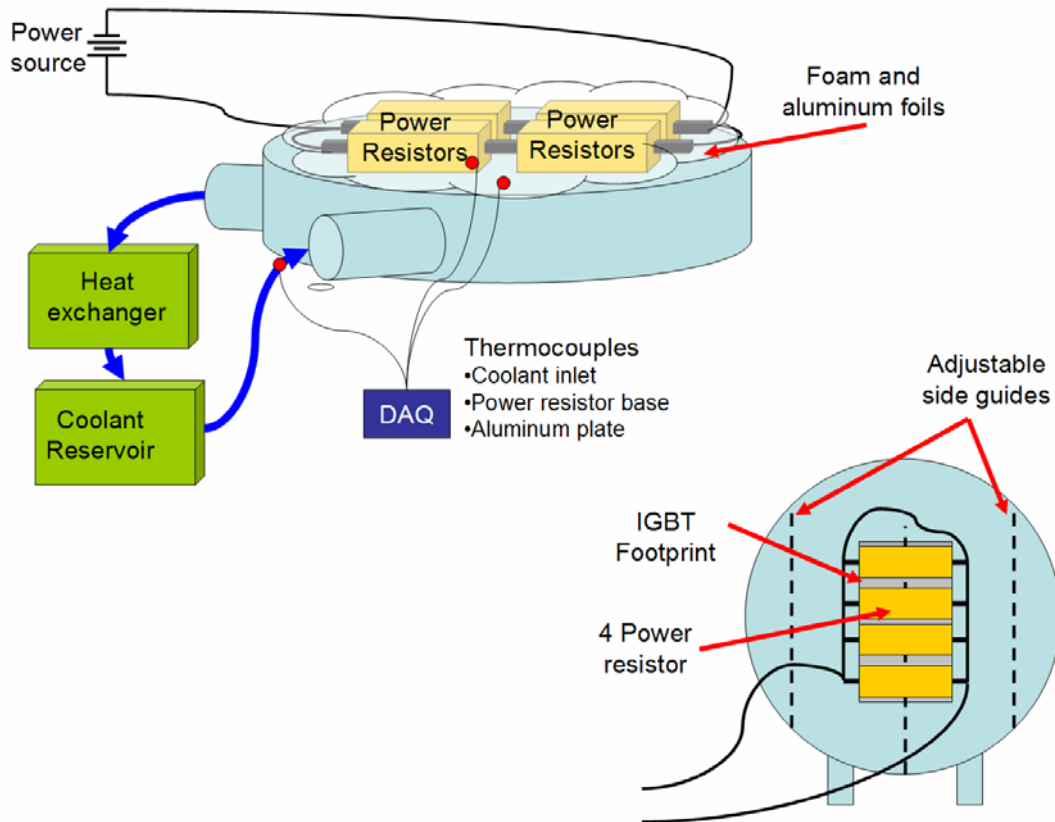


Figure 10: Heat sink test setup design with power resistors

The heat sink is connected to a cooling loop as would be found in an automotive system with a pump, a reservoir, a radiator and fans. The resistors are electrically combined in such a way that with the 24V source approximately 600 W are dissipated. The resistors are pressed against the heat sink, so that they occupy the IGBT footprint. They are wrapped in insulation and aluminum foil so that the dissipated heat has to be absorbed by the coolant for the most part. Thermocouples are placed in the coolant flow at the inlet, on the heat sink aluminum plate and on the power resistor base.

4.6.2 Test setup

The test setup is pictured in Figure 11. The heat sink is an open cylinder with inlet and outlet. The plastic cover offers insight to the chamber and grants easy access to replace guides for different setup. The guides are small machined aluminum strips that fit in the chamber.

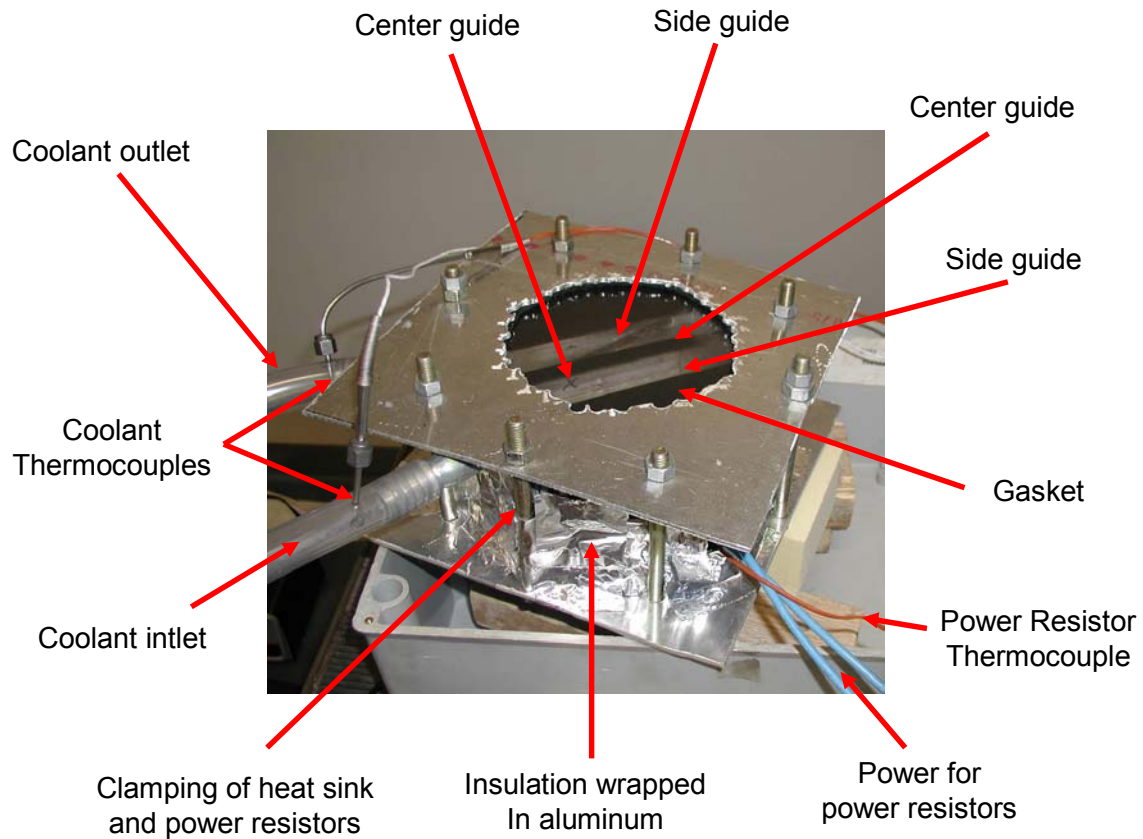


Figure 11: Heat sink with adjustable guides and the power resistors for testing

The resistors are pressed against the heat sink through a tie rod system, which also hold a gasket and the guides tightly in place. Fiberglass insulation is placed around the resistors and an insulating piece of wood is placed between the resistors and the tie rod system.

The entire test stand is pictured in Figure 12. The heat sink with the power resistors are at the top of the stand. Most of the coolant loop is located on the left side of the stand. The power supply for the resistors takes most of the lower part of the setup. Finally the instrumentation is mainly located on top of the table in the form of multimeters.

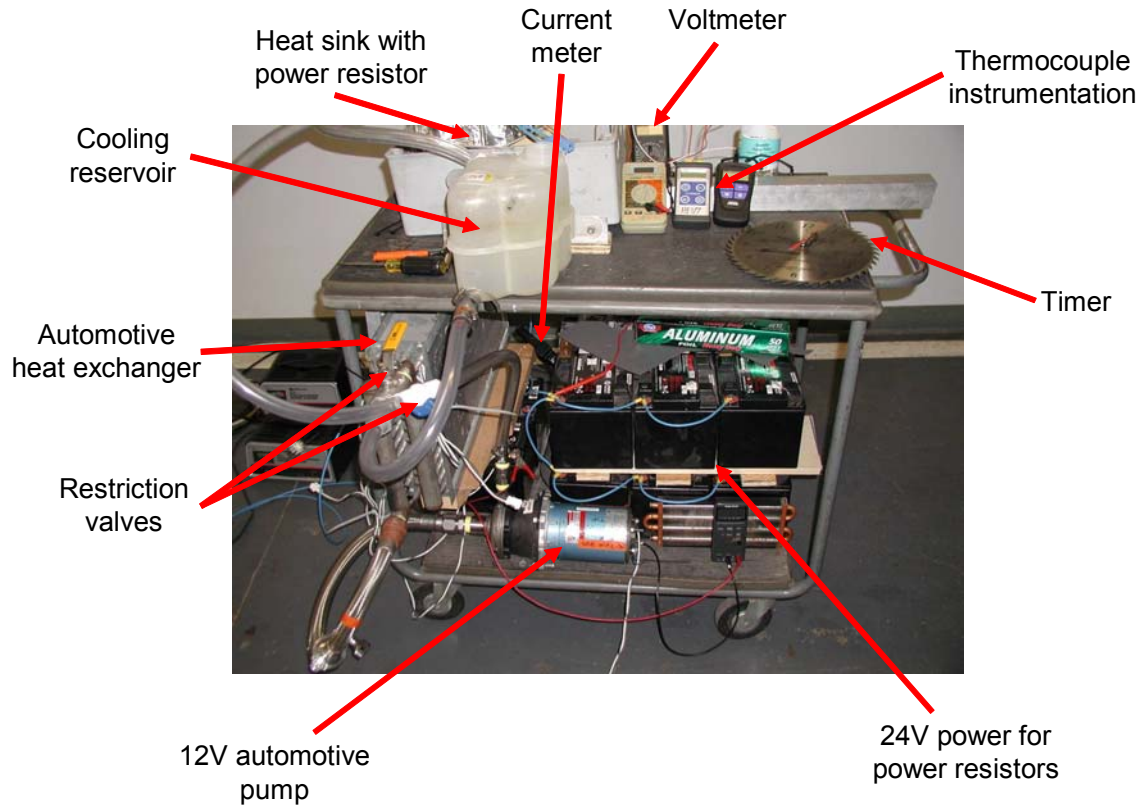


Figure 12: Entire test setup for heat sink with power resistor

The coolant loop is driven by a large 12 V automotive pump. In order to achieve the 3 gpm of flow, a restriction valve was used. This valve put back pressure on the pump to reduce the flow. The flow could be reduced to about 4 gpm. The rest of the loop is standard automotive components including a reservoir, which helps eliminate the bubbles, and radiator-fan combination as used in vehicles.

The power resistors are pressed against the heat sink. These resistors get powered through 12 V 42 Ah lead acid batteries. This provides a good power source for the resistor. Very little voltage drop occurs during tests. The batteries are connected in such a way that the voltage is 24 V, which dissipates about 600 W with appropriate resistor arrangement and also prevents damaging the resistors. The voltage feed to the resistors is read using a multimeter. The current going through the resistors is measured using a clamp current probe. The product of the two measurements equals the heat dissipated in the power resistor.

The three thermocouples are in the locations as indicated in Figure 10. Thermocouple readers are used to display the temperatures. Before each test, the batteries were charged while the coolant loop was turned on to allow all temperatures to reach a steady state. Once the batteries were charged and all temperatures were constant, the power resistors were connected to the power source. All the voltage, current and temperature readings were recorded every 15 seconds by hand. After temperatures reached steady values, the

power resistors were disconnected from the batteries. The logging of data was continued until the temperatures reached close to their steady state temperatures.

4.6.3 Heat sink power resistor testing results

Figure 13 represents a typical data set from the heat sink testing with power resistors between 605 W and 597 W.

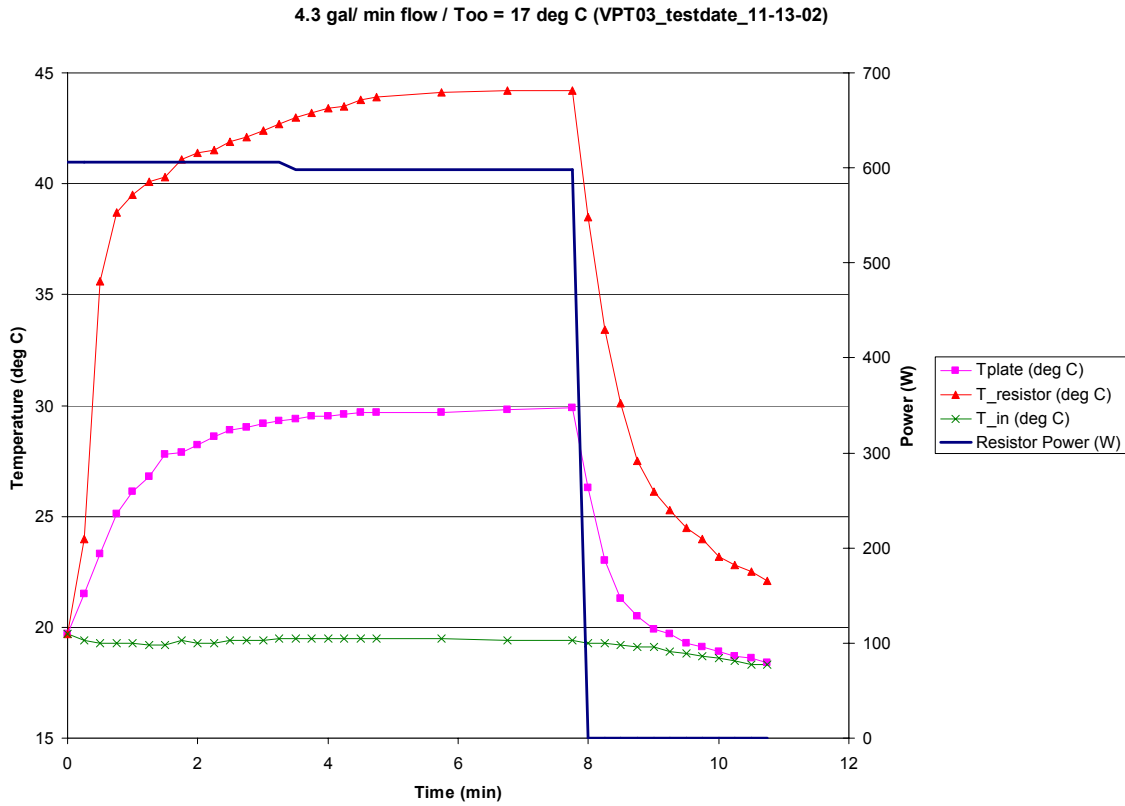


Figure 13: Results from heat sink testing with power resistors

As the blue power curve shows the power resistors were dissipating 600 W according to the scale on the left side. This graph also shows that the batteries deliver a constant power over the test. The temperature rise is pretty immediate for the power resistors and the heat sink plate. The power resistor experiences a temperature rise of 25 deg C and the aluminum plate temperature steadies out after a rise of 10 deg C. After 8 minutes the power resistors are turned off and the temperature immediately drops as expected.

This test was made to verify that the original design concept will meet the specifications. Therefore this high power test was performed. The high power level generates good temperatures differences allowing the data to come out of the noise level.

4.7 Cold chamber calculations

4.7.1 Mathematical model

The coolant flow in a pipe is a classic heat transfer problem and therefore the solution is well established. The model of the cold chamber presents more challenges. To approximate the cold chamber geometry, it is decomposed into smaller sections and each rectangular section is transformed into a classic pipe section using hydraulic diameters.

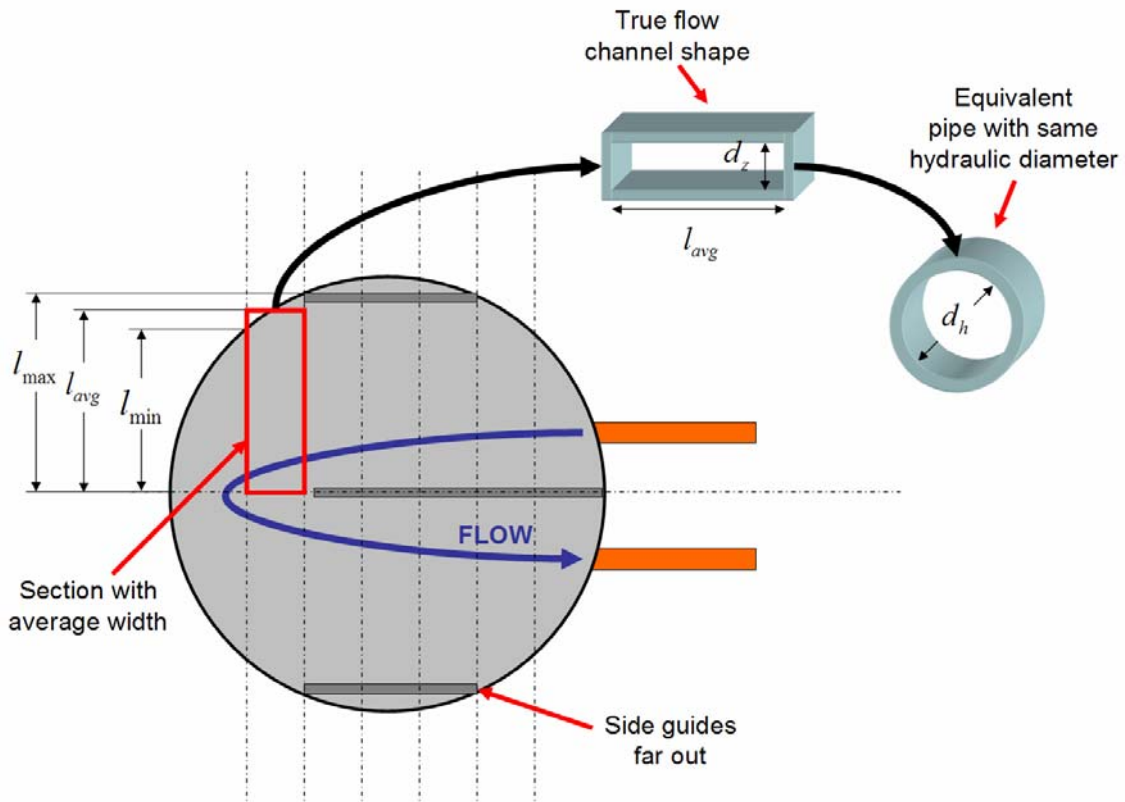


Figure 14: Mathematical cold chamber approximation

The hydraulic diameter is based on having the same cross-sectional areas for the flow as shown in Equation 4. The hydraulic diameter is simply defined in

Equation 6.

$$A_{\text{rectangular}} = A_{\text{circular}} \quad \text{Equation 4}$$

$$l_{\text{avg}} d_z = (d_h)^2 \pi \quad \text{Equation 5}$$

$$d_h = \sqrt{\frac{d_{\text{avg}} d_z}{\pi}} \quad \text{Equation 6}$$

On each section, heat transfer, initial temperatures, ending temperatures, and checks for turbulent flows, are calculated and these calculations are propagated through the entire chamber. This approximation allows for the different positions of the side guides and accounts for the sections that are rounded.

Using the section approximation and the convection heat transfer from Equation 2, a computer model can be established.

4.7.2 Computer model

The equations are coded in Matlab. The code is shown at the end of Appendix 2. The code uses a base heat transfer function called “pipe_heat.m”. It computes the heat convection in a pipe as described in Appendix 2. A high level function called “heatsink.m” decomposes the chamber into the small section using the hydraulic diameter and then computes the heat transfer for each section.

4.7.3 Design insights and decisions based on modeling

The model allows inspection for individual sections and their characteristics. Figure 15 presents a case study with detailed results for each section.

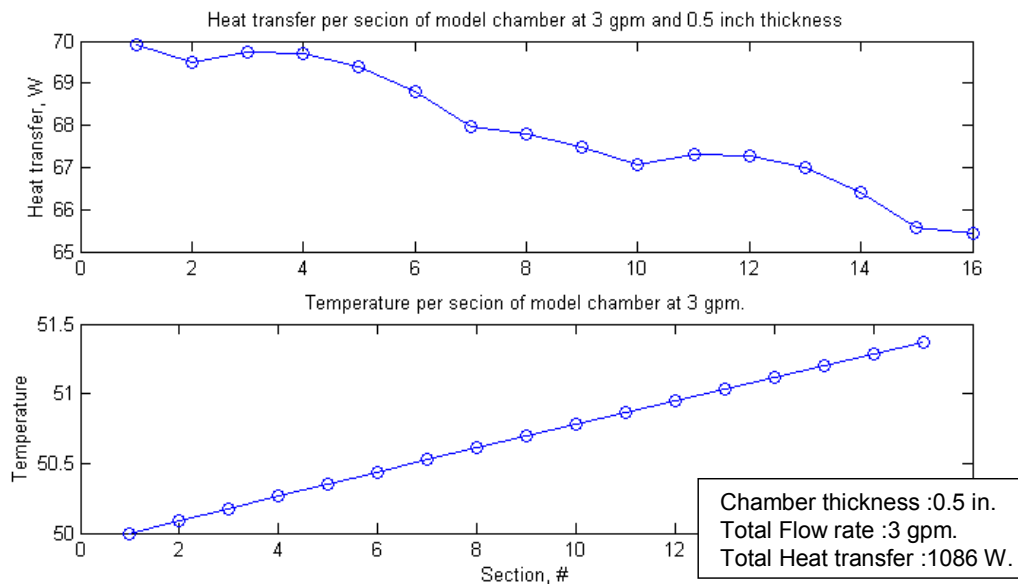


Figure 15: Half inch cold chamber thickness case study results (based on a 20 deg C temperature differential)

The cold chamber was divided into 16 sections. The figure clearly shows the contributions from the different sections even though heat flux is higher. The smaller sections dissipate less heat due to their smaller surface area compared to the larger

sections. The temperature increase is pretty linear throughout the sections. Therefore the sections at the exit of the heat sink present less heat dissipation since the temperature difference is smaller.

Another design factor is the thickness of the heat sink. The thickness affects the mass of coolant in the chamber and the flow velocity which both affect the heat transfer capabilities. Figure 16 shows the possible heat transfer as function of heat sink thickness and the flow rate.

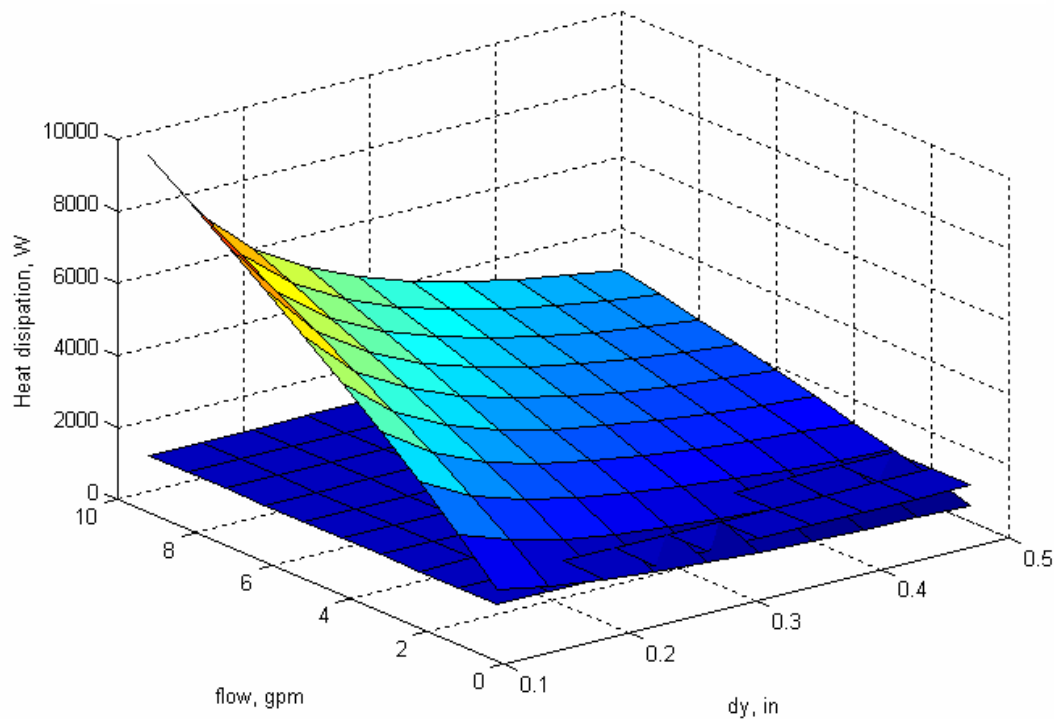


Figure 16: Cold chamber heat dissipation as a function of chamber thickness and coolant flow rates (based on a 20 deg C temperature differential)

All these calculations are based on steady state iterations. The model allows the flow to be laminar for the calculations of the heat transfer coefficient, but in reality the inlet expansion ruptures any laminar flow in the chamber. During the 1 gpm case the flow in some section was close to laminar. Turbulence allows for a greater heat transfer coefficient so this model predicts the worst case scenario.

Standard flow rates on electronics in electric and hybrid vehicles are about 3 gallon per minute. The thickness is determined by the physical setup. The fittings to feed to the chamber need to fit in the heat sink as well. Therefore half inch thickness was selected. The model predicts a heat transfer of 1500 W at those operating points.

4.7.4 Testing data compared to model

Figure 17 shows the model results along with the data from the power resistor setup shown in Figure 13. As predicted the model shows higher temperatures and the conservative nature of the model is confirmed. The model levels out but the real system keeps increasing. This model does not incorporate a radiator system, but instead uses a coolant with constant inlet temperature.

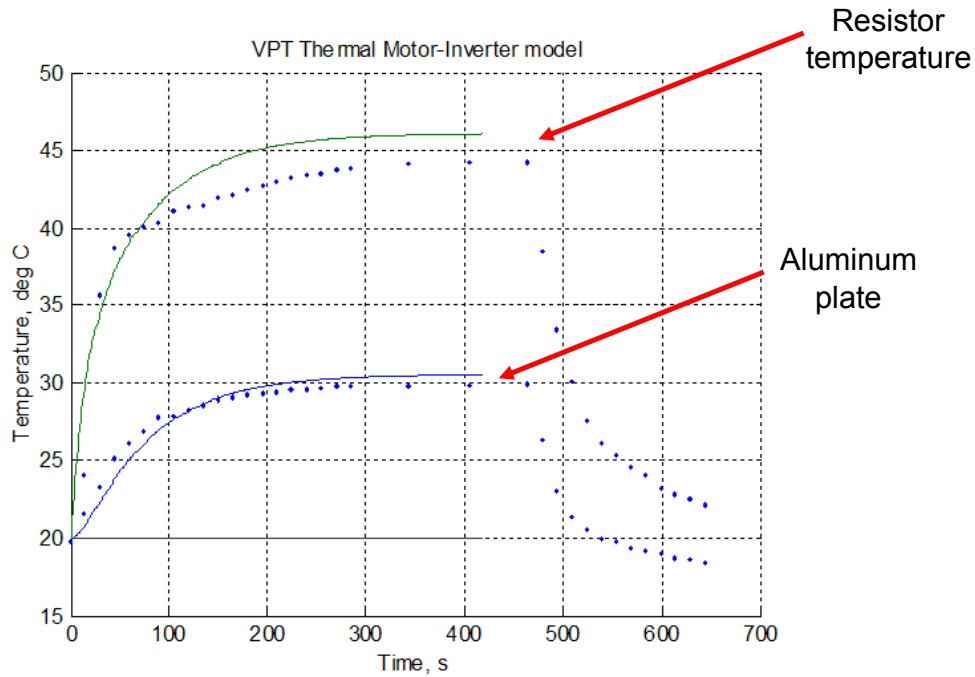


Figure 17: Heat sink test data compared to the model

4.8 Final design

The final design is a heat sink designed to cool the power electronics and the motor with a flow rate of 3 gpm of coolant. Figure 18 shows the final design of the heat sink. The channels are made out of a bent sheet of steel. The piece of steel has a double function, besides forming the flow channel; it is a shield for the power electronics to be protected from the electromagnetic source from the motor. Since the rest of the case is aluminum and aluminum does not affect magnetic fields, the steel plate is needed.

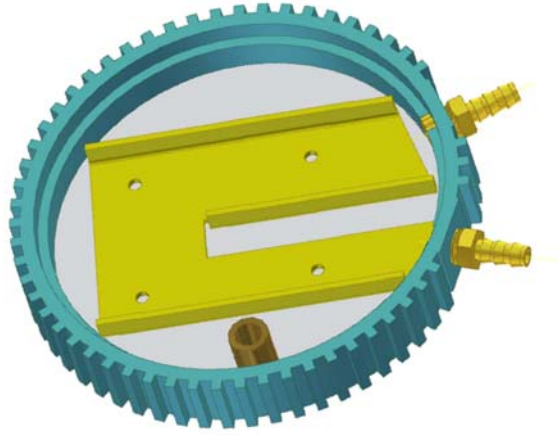


Figure 18: Final heat sink design

5 The thermal model of the motor inverter assembly

5.1 The motor and inverter assembly

The unit is composed of the motor and the inverter. So far the inverter part had the focus. The thermal component of the inverter is the IGBT. The motor has significantly more parts. The rotor and the stator are the major thermal components. The stator is broken into its different materials, as well as the core and the ends of the windings. The other thermal masses of the motor are the bearings, the casing pieces and the shaft. Figure 19 illustrates and lists the thermal masses which compose the motor inverter unit.

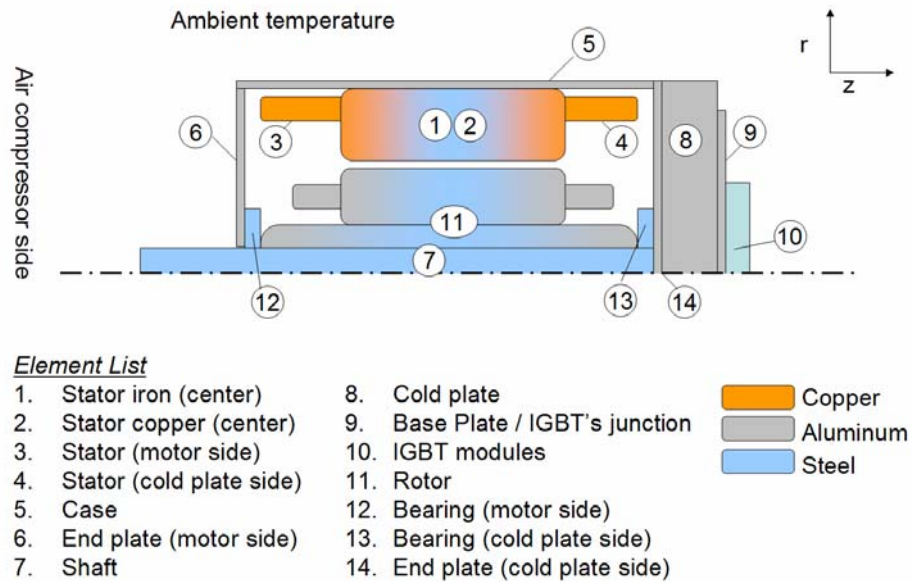


Figure 19: Thermal mass composing the inverter-motor unit

Table 3 lists the specifications of the lumped masses.

Table 3: List of the thermal masses and their specification

Mass label	Description	Medium	Mass (kg)
M1	Stator iron (center)	Steel / Copper	3.856
M2	Stator copper (center)	Copper	3.682
M3	Stator (motor side)	Copper	3.682
M4	Stator (cold plate side)	Copper	3.682
M5	Case	Aluminum	4.069
M6	End plate (motor side)	Aluminum	0.368
M7	Shaft	Steel	0.052
M8	Cold plate	Aluminum	1.214
M9	Base plate / IGBT's junction	Aluminum	0.368
M10	IGBT modules		0.136
M11	Rotor	Aluminum / Steel	4.173
M12	Bearing (motor side)	Steel	0.683
M13	Bearing (cold plate side)	Steel	0.683
M14	End plate (cold plate side)	Aluminum	0.368

5.2 Lumped capacitance model and validity

The lumped capacitance method is the simplest and most convenient method to solve the thermal development within the motor. The thermal masses defined above are all metals with high conductivity (k) from 65 to 150 W/mK. The convection from the air with the case is low. The convective coefficient is about 25 W/m²K, since free convection is assumed to generate conservative estimates. The highest Biot number is about 0.05. Therefore the temperatures across the lumped masses can be approximated to be constant.

The lumped capacitance model is a meaningful model to use, since the temperatures of the lumped masses should be constant through out the masses. But this is an assumption that might not always be true.

5.3 Explicit finite difference method

Finite difference is used in the model as explained in Fundamentals of Heat and Mass Transfer (*Incropera, 1996*).

The fully explicit method is chosen over the implicit to simplify the computations. In the explicit finite difference method all temperatures are computed only based on temperatures of the prior time step. This induces the possible occurrence of instability. To avoid computational instability, the time step needs to be small enough. This can impact the computation time and increase it drastically.

So for example the temperature of the right stator end is defined by Equation 7. The temperature differences divided by the resistances represent the heat flows between the different lumped masses. Notice that all the temperature are based on the prior time step. The calculation also incorporates the heat generation within the lumped mass. Finally the

temperature of the lumped mass is based on the net sum of the energy flows (terms in parenthesis), the thermal capacity and the time step.

$$T4_{t+1} = \frac{dt}{m4 \cdot c4} \left(\frac{T1_t - T4_t}{R14} + \frac{T2_t - T4_t}{R24} + \frac{T5_t - T4_t}{R45} + \frac{T14_t - T4_t}{R414} + qgen4 \right) + T4_t \quad \text{Equation 7}$$

5.4 The thermal resistance network

The lumped mass capacitance model views the masses as thermal capacitances connected by a resistor network. The resistors represent the thermal paths. The thermal network for the motor inverter unit is presented in Figure 20. The lumped masses are represented by the number assigned in Figure 19.

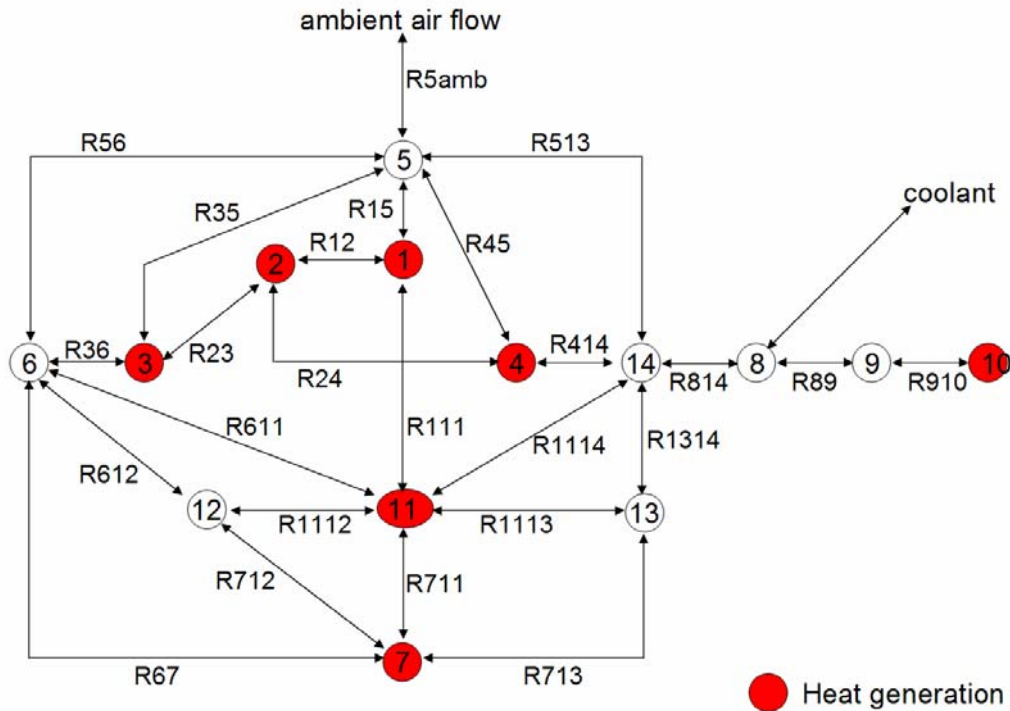


Figure 20: Thermal network for the motor inverter unit

The lumped masses highlighted in red generate heat. The heat generation is mainly due to ohmic losses in the windings in the motor. The stator generates the most heat in the high current copper windings. The rotor also experiences heat generation due to induced currents. In the inverter the IGBT is the heat generator due to switching and conduction losses.

The thermal paths represented are conduction, convection, radiation and combinations of the above.

5.5 Dimensions for the modeling

The thermal resistances are defined by the geometry and the dimensions of the assembly. Figure 21 illustrates the dimension definition of the inverter motor assembly. The dimensions are defined by two vectors. The axial direction and the radial direction are used.

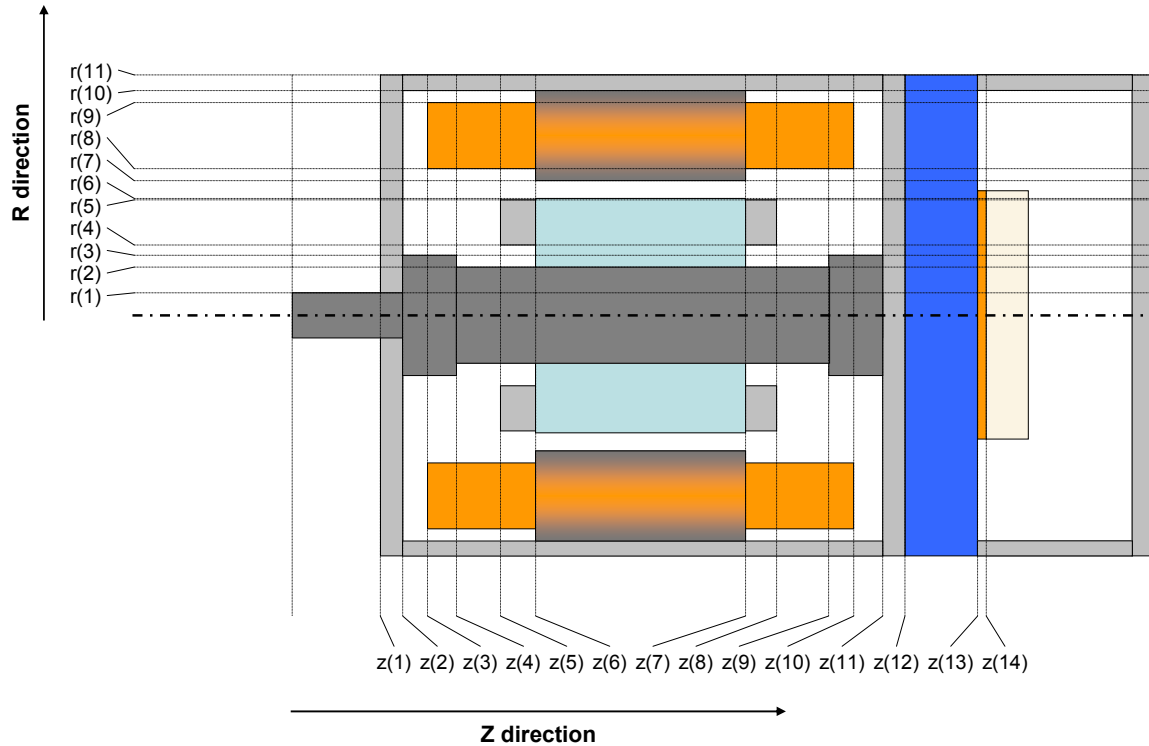


Figure 21: Dimension of the assembly for the model

5.6 Computation of the thermal resistances

The thermal resistances in the resistive network are defined by the physical system. The three modes of heat transfer are conduction, convection and radiation. Each resistance is a combination of the above, based on the physical layout. So for example mass 9 and mass 10 only have conduction and only the conduction is defining the thermal resistance.

Let's investigate the thermal resistance between the motor casing and the environment as detailed in Equation 7. The first heat transfer path is the conduction in the aluminum casing to the outside edge. Next, convection with the environment takes place and is represented with a convective heat transfer coefficient. Finally, radiation is considered.

$$R_{4amb} = \frac{dz_{4/2}}{k_{al} \cdot a_{4amb}} + \frac{1}{h_{4amb} \cdot a_{4amb}} + \frac{1}{\text{sig}_{4amb} \cdot \text{emis} \cdot (T_{amb} + T_4)(T_{amb}^2 + T_4^2)} \cdot a_{4amb}$$

Equation 7

Each thermal resistance is defined in Appendix 3.

5.7 The thermal model computational flow

5.7.1 Overview

The code is composed of 3 stages. First a setup defines the physical system, the initial conditions and the operating conditions. The second part is the heart of the code, the explicit finite difference code which computes temperatures over time. Finally the code creates figures to analyze the results. Figure 22 illustrates the flow of the code to the thermal model.

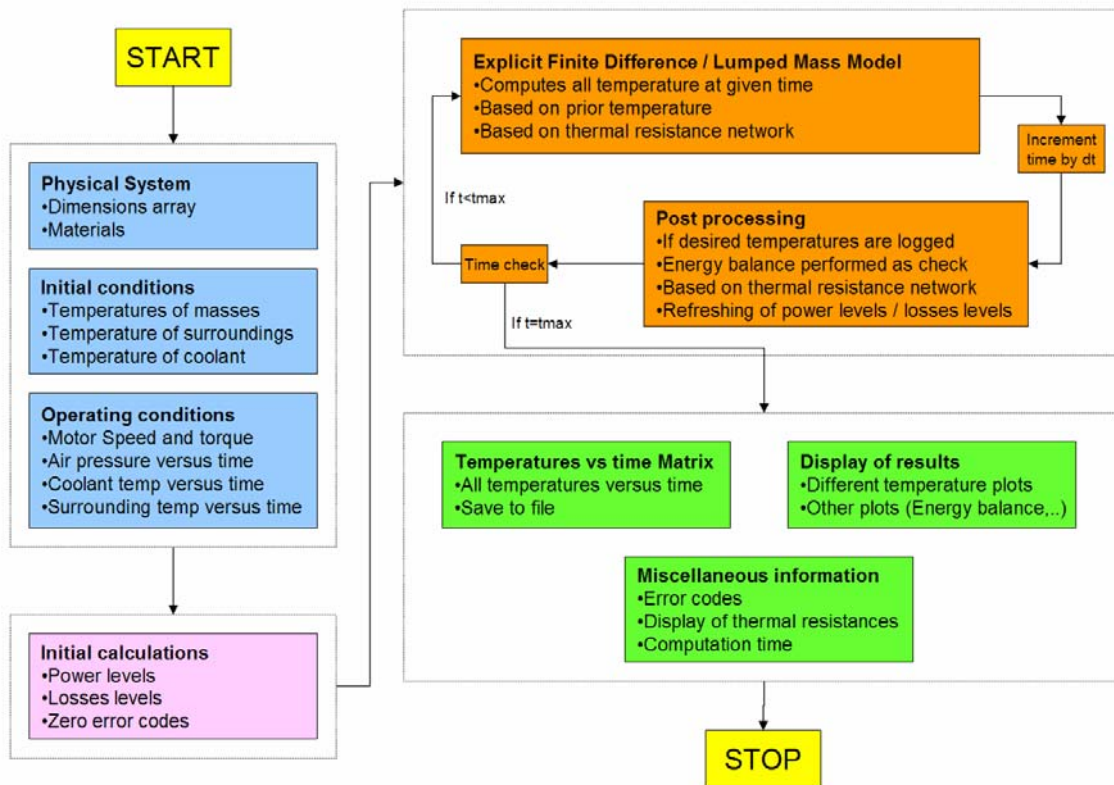


Figure 22: Flow of the thermal model computation

The model geometry is defined for the VPT motor. The input to the model is shaft power and rpm. The output is an array of the temperatures of all the lumped masses versus time.

5.7.2 Setup for the code

The setup defines the base parameters such as the time step of the computation, the computation length and the temperature storage period. The time step determines the stability of the iterations. To help the computation time, the temperatures are only stored periodically, rather than at every iteration, thus freeing memory for computation.

The initial temperatures are defined for each mass. These are usually set to ambient temperature.

Next the physical properties and geometric properties are defined. The thermal resistances are computed one by one. Finally the thermal capacitance of each lumped mass is computed.

The operating conditions defined the internal losses of the components. A look up table assigns heat generation numbers to the lumped masses based on data available from prior research. Dr. Konrad established a table of losses this motor design as shown in Table 4.

Table 4: Losses in the different motor and inverter constituents

Speed (RPM)	Torque (nm)	Stator Cu Ws loss	Rotor Cu Ws loss	Iron Loss (Ws)	Stray Loss (Ws)	IGBT (Ws)	Efficiency (units)	Pwr Out (Ws)
0	10.46	157.1	88.9	0.4	0.0	0.0	0.0	0.0
1000	10.35	157.1	88.2	13.2	3.1	7.9	80.5	1082.8
2000	10.30	157.1	87.8	32.7	8.6	15.8	88.3	2154.2
3000	10.26	157.1	87.5	56.6	15.6	23.7	91.0	3218.3
4000	10.22	157.1	87.3	84.1	23.8	31.6	92.4	4276.4
5000	10.19	157.1	87.1	114.7	33.2	39.5	93.1	5329.3
6000	10.16	157.1	86.9	148.0	43.4	47.4	93.6	6377.7
7000	10.14	157.1	86.7	183.9	54.6	55.3	93.9	7421.9
8000	10.11	157.1	86.5	222.1	66.5	63.2	94.1	8462.3
9000	10.08	157.1	86.4	262.6	79.2	71.1	94.2	9499.0
10000	9.89	157.1	92.0	266.4	98.7	78.9	94.4	10345.3
11000	9.32	157.1	99.7	246.1	123.4	86.8	94.5	10733.1
12000	8.68	157.1	103.8	235.3	146.4	94.7	94.4	10908.2
13000	8.09	157.1	106.3	228.8	169.2	102.6	94.3	11002.4
14000	7.54	157.1	108.4	224.4	192.8	110.5	94.2	11060.0
15000	7.07	157.1	110.0	221.5	217.0	118.4	94.0	11093.5
16000	6.64	157.1	111.4	219.6	242.0	126.3	93.8	11108.5
17000	6.24	157.1	112.5	218.4	267.6	134.2	93.6	11108.9
18000	5.89	157.1	113.4	217.7	294.0	142.1	93.4	11097.5
19000	5.58	157.1	114.2	217.3	321.0	150.0	93.2	11076.3
20000	5.28	157.1	114.8	217.1	348.7	7.9	92.9	11046.6
21000	5.01	157.1	115.4	217.2	377.1	15.8	92.7	11009.7

The torque speed curve is based on driving an air compressor for an assumed flow and pressure versus fuel cell stack current.

All these parameters are stored in matrices. This allows for easy passing of variable and flexibility in the programming. Now the program is feeding into the finite difference loop.

5.7.3 Explicit finite difference structure

The finite difference structure is called by the function 'finitedifference.m'. It contains a time loop in which at each time step the heat sink absorbed energy is computed. The energy absorbed is computed using the theory and code developed in section 4. This absorbed energy is assigned as outgoing energy to the heat generator term in the heat sink.

Then the lumped mass function is called in 'lumpedmassloop.m'. Once all the temperatures for the next time step are calculated they are reference to become the old temperature for the next time iteration.

The lumped mass function computes the temperatures of each lumped mass based on old temperatures, the thermal capacities and the thermal resistive network by calling 'explicitenergybalance.m'.

Figure 23 illustrates the structure used to program the difference method.

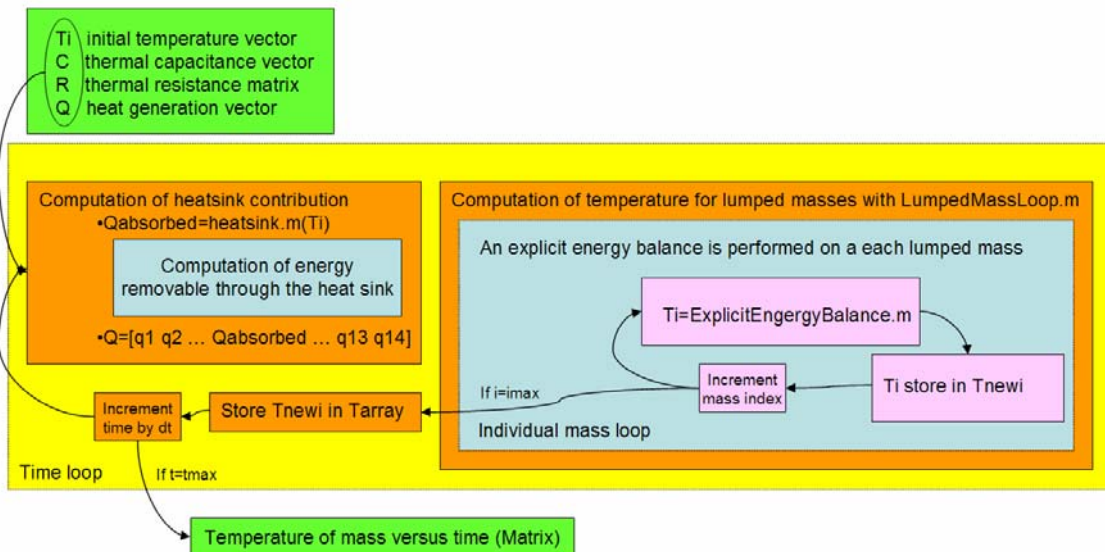


Figure 23: Finite difference code structure

Other features include an energy balance which stores the energy input and output to the system so that an energy balance can be performed in the end. Some error flags are set in the program if the input data contains unreasonable values or if the computation becomes unstable.

5.7.4 Outputs

Several short functions can be used to plot temperatures versus time or store the temperature in a tab delimited file. The overall energy balance is verified and other information is provided such as the overall computation time.

6 Inverter testing with power electronics

6.1 Test set up

6.1.1 Instrumentation plan and implementation

The inverter-motor unit is instrumented with type K-thermocouples. The locations of these thermocouples are shown in Figure 24. The majority of the measurements are close to the IGBT and the heat sink itself.

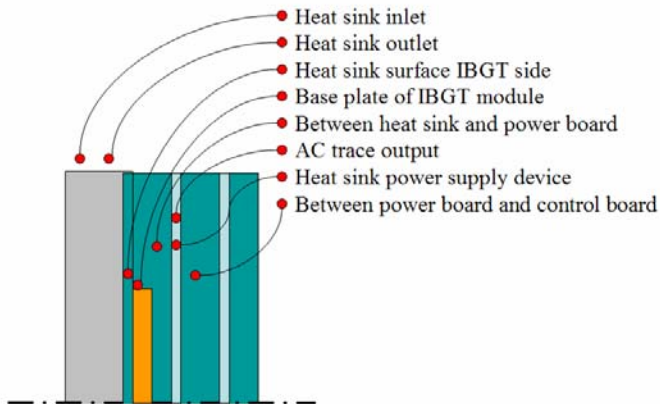


Figure 24: Schematic showing the thermocouple placements on the inverter

The thermocouples on the inverter unit monitor the IGBT base plate temperature, the coolant temperature rise, the aluminum heat sink plate temperature, as well as a few other heat sensitive components. The instrumented IGBT and heat sink is shown Figure 25.

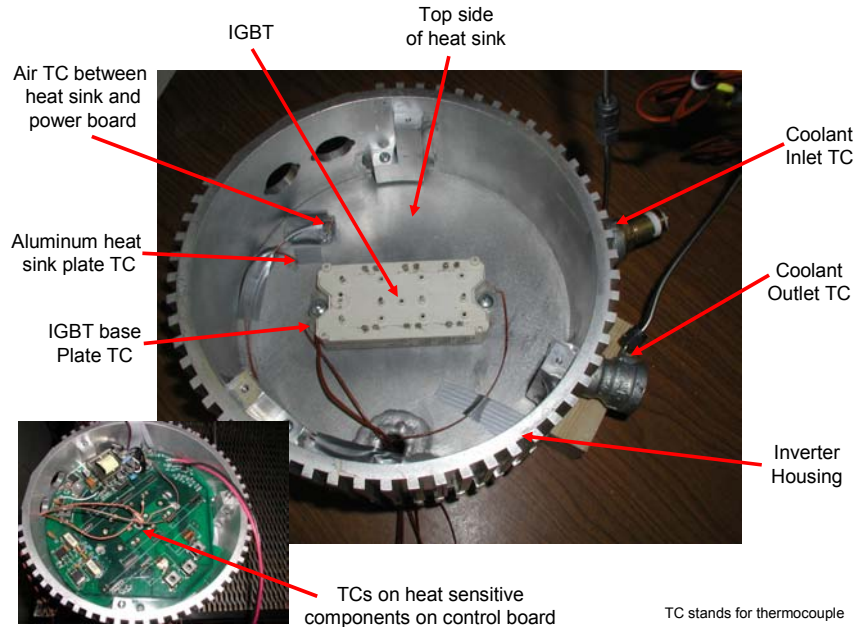


Figure 25: Instrumentation of the heat sink and inverter

The thermocouples at the coolant inlet and outlet of the heat sink are used to calculate the energy absorption of the coolant. The IGBT and aluminum plate thermocouples track the energy transfers during operation and will validate the thermal model.

6.1.2 CPES test facility

In this test, only the inverter unit was tested. The thermal tests were only secondary to correct functioning of the power electronics, since the gate drive circuit designed by Chris Smith needed to be tested and improved as a priority. The test was setup in CPES (Center for Power Electronic Systems) at Virginia Tech. Figure 26 presents the test facilities as well as the equipment used.

In CPES, the thermocouples were run to an ‘HP 34970A Data Acquisition / Switch Unit’. This unit interfaces with a laptop that runs the HP specific software. The software allows real time visualization of the temperatures. Thus at all times the testing could be terminated if the temperature would rise to unacceptable levels. The unit would also log data in a tab delimited text file.

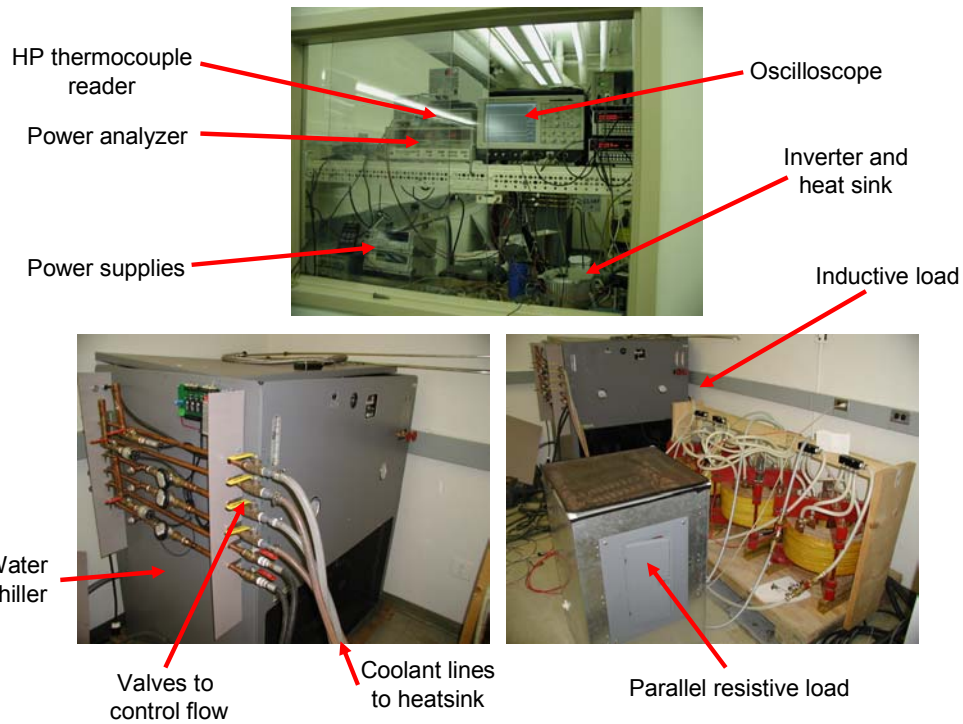


Figure 26: CPES testing facility

The inverter was in a test cell along with the instrumentation. The inverter is connected to an inductive load in parallel with a resistive load to simulate the motor windings. The inductive load was composed of three variable value inductors. Each inductor represented a phase. The inductors were set to simulate the inductance of the motor windings. The resistive load in parallel was made of power resistors packaged in a shroud with a fan providing convective cooling. The heat sink was connected to a water chiller. The flow rate was controlled by using the valves on the chiller.

6.1.3 Test procedures

For the thermal test, the IGBT is switching at higher power rates. The power analyzer readings determine the losses within the IGBT. That power loss number is used for the model. The tests were run until temperatures reached steady state or the temperature level was too close to operating limits on components.

6.2 Experimental Results

Figure 27 presents the temperature readings for the inverter testing in CPES. Two different flow rates for the coolant were run: 3 gallon per minute and 2 gallon per minute.

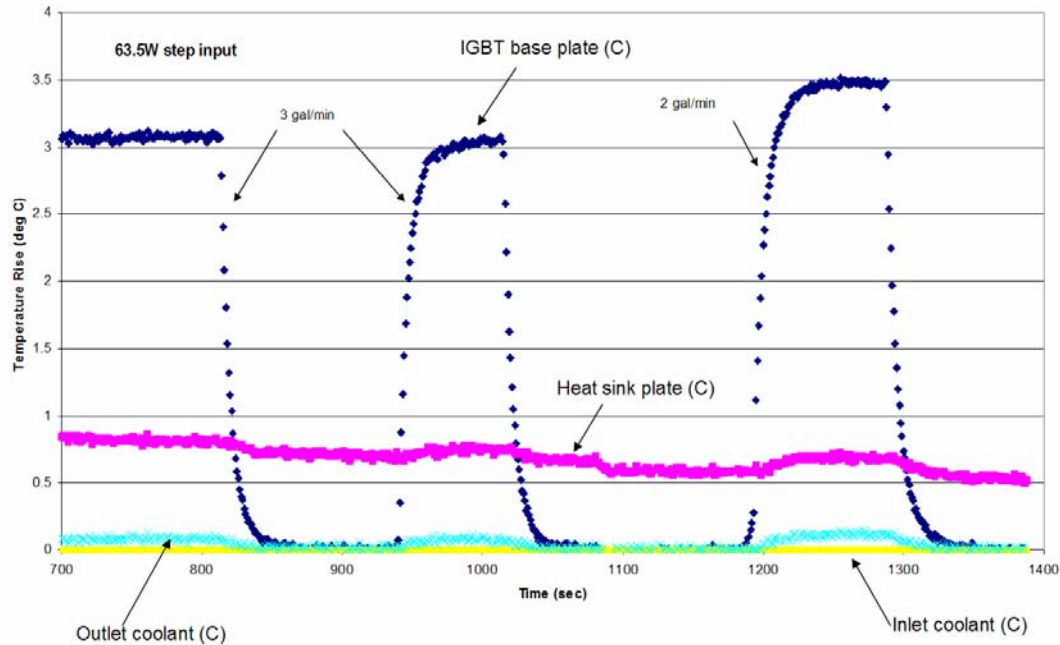


Figure 27: Inverter testing results at CPES

The 63 W of losses induced a 3 deg C temperature rise in the IGBT base plate at 3 gpm coolant flow. The temperature rise in the coolant is close to insignificant. But the coolant exit temperature raises more with slower coolant rate as one would expect.

The thermocouple measuring the Al plate of the heat sink is further away from the base plate. The thermal mass is large enough to keep it temperature relatively constant over the short transients. This also shows the limitation of the lumped mass model, the temperature across the aluminum in the heat sink is not homogenous, but close to constant in space.

6.3 Comparison to the model

The same conditions were entered into the model and the case computed. The results are shown in Figure 28.

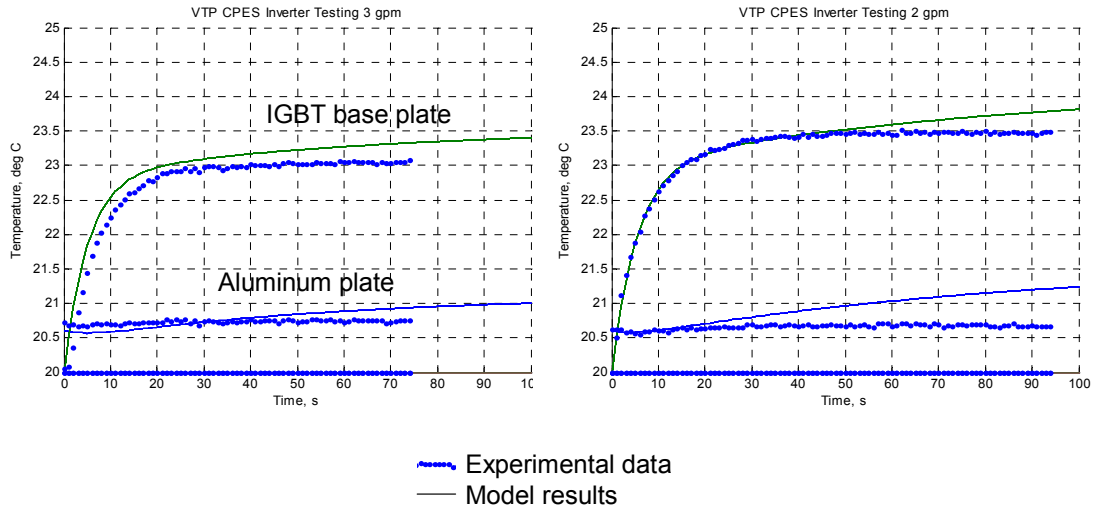


Figure 28: Temperatures computed by the model for the CPES test

The model presents the right time constants. The data of the 3 gallon per minute test was used to calibrate the contact resistance between the Aluminum plate of the heat sink and the IGBT copper base plate. The 2 gallon per minute test returned computed temperatures that match the real data. This proves the validity of the heat sink inverter model.

Since the thermal capacity of the chiller in CPES is unknown, the model assumes an infinite coolant reservoir, thus the coolant temperatures is constant. The model temperatures are still rising, although the empirical data has reached steady state.

6.4 Conclusion and model adjustments

For this test a real IGBT was used, therefore the contact resistance and the footprint generating the contact resistance are now calibrated. The model generates temperatures that match empirical data.

7 Motor Inverter Assembly

7.1 Test Setup

7.1.1 Instrumentation of the unit

Figure 29 illustrates the thermocouple location for the entire motor inverter assembly. One important measurement is the copper winding temperature. The case temperature also presents important information on the convection heat losses of the unit. Ideally the temperature measurements would cover all the thermal masses. Unfortunately it was not possible due to technical reasons. The goal was not to damage the motor, the inverter or the casing.

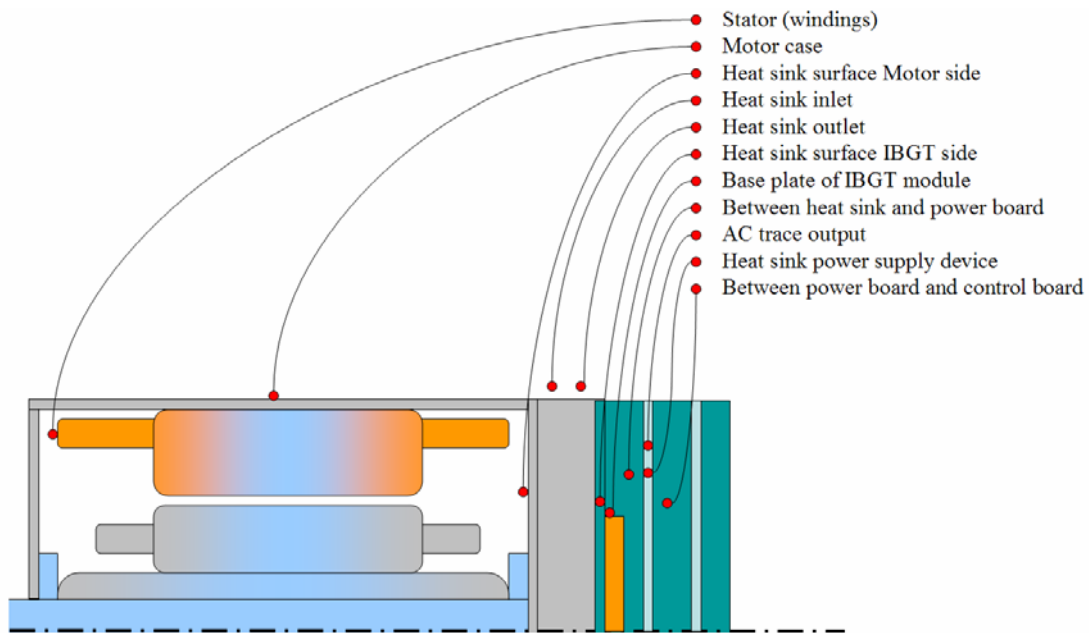


Figure 29: Motor inverter instrumentation plan

The inverter was instrumented just the same as in the test presented in section 6 (cf Figure 25). A thermocouple on the casing and the end plate were easily installed. The mounting of the stator thermocouple is illustrated in Figure 30.

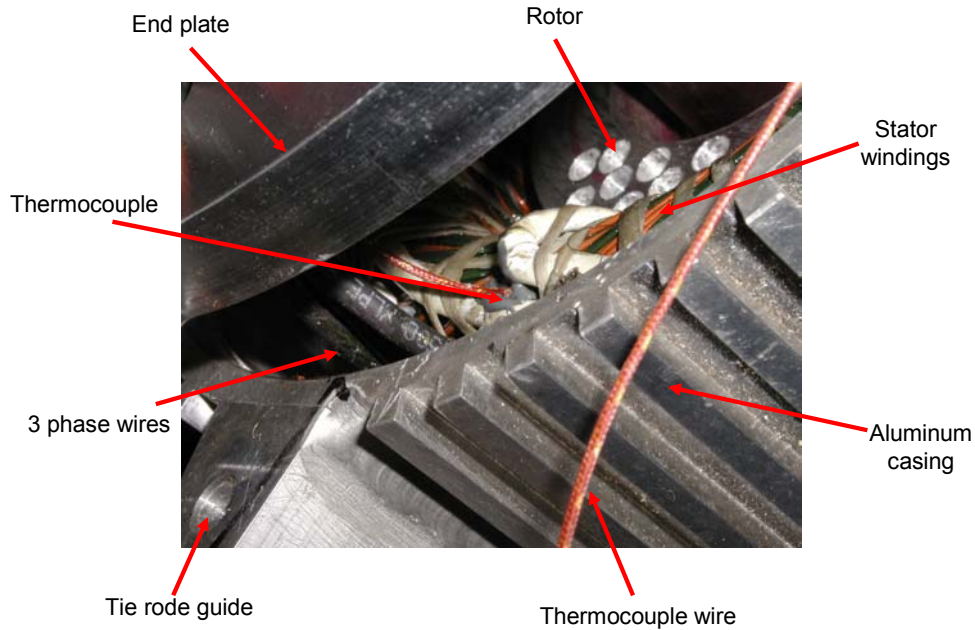


Figure 30: Motor instrumentation

The data acquisition system for the thermocouples was different. A National Instruments FieldPoint Module with a thermocouple block was used. The interface was a Virtual Instrument written in Labview. The temperatures are displayed on the screen and update in real time. In the background, all the temperatures are carefully logged every second.

7.1.2 Test Stand with Air Compressor

For this test of the entire unit, the motor inverter unit is coupled to an actual air compressor as shown in Figure 31. The compressor is typical in fuel cell applications. To simulate the fuel cell pressure drop, a throttle valve is plumbed to the exit of the compressor. The inverter is powered from a high voltage battery pack. The pack is composed of 28 lead acid batteries as used in fuel cell and hydrogen engine generator electric hybrid vehicles at Virginia Tech. The voltage and the current draw on the battery pack is measured which allows an estimate of the power level of the motor inverter assembly. The motor speed is controlled through a small interface box. The monitoring of the motor is performed with EMPCON (Embedded Power Controls Inc) interface software.

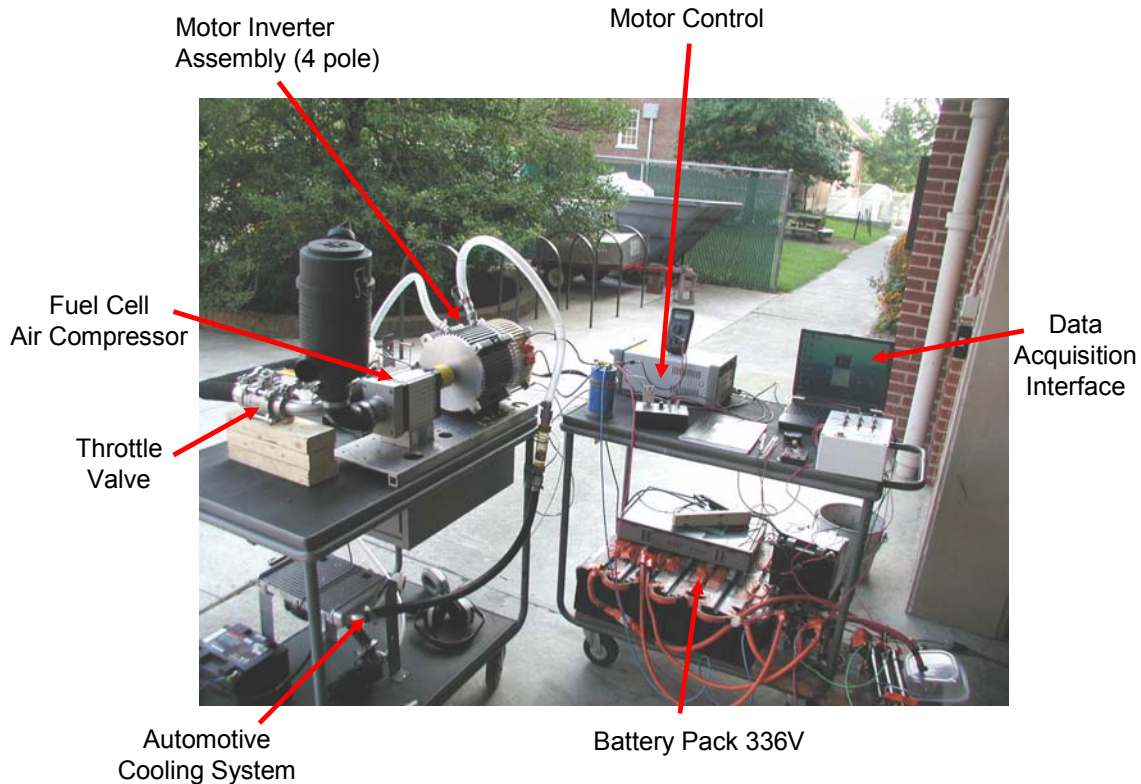


Figure 31: Air compressor testing setup

The cooling system is also built with components similar to those used hybrid vehicles. A 3 gallon per minute pump is powered by a 12V battery. A reservoir feeds the pump with coolant. The pump pushes the coolant through small heat exchanger (built for an ATV). An electric fan is mounted to the heat exchanger and powered at all times by the 12V battery. A flow meter is inline before the coolant enters the heat sink. From the heat sink, the coolant is recycled to the reservoir.

The major limitation of this coolant system is the lack of ram air. The fan can not push as much air through the heat exchanger as driving at high speeds. From experience on hybrid vehicles that is a major difference. The temperature monitoring was used to ensure that no component sustained any damage.

The twin screw compressor made by Opcon is plumbed to a throttle valve. The air intake is filtered to prevent any particles from damaging the screws. The compressor is loaded by closing the throttle at the exit. The exit of the compressor is instrumented with a pressure gage and thermocouple. The exit air pressure and temperature along with the compressor speed determines a given power output from the electric motor at the shaft.

Figure 32 provides a closer look at the air compressor coupling to the motor as well as the plumbing around the compressor.

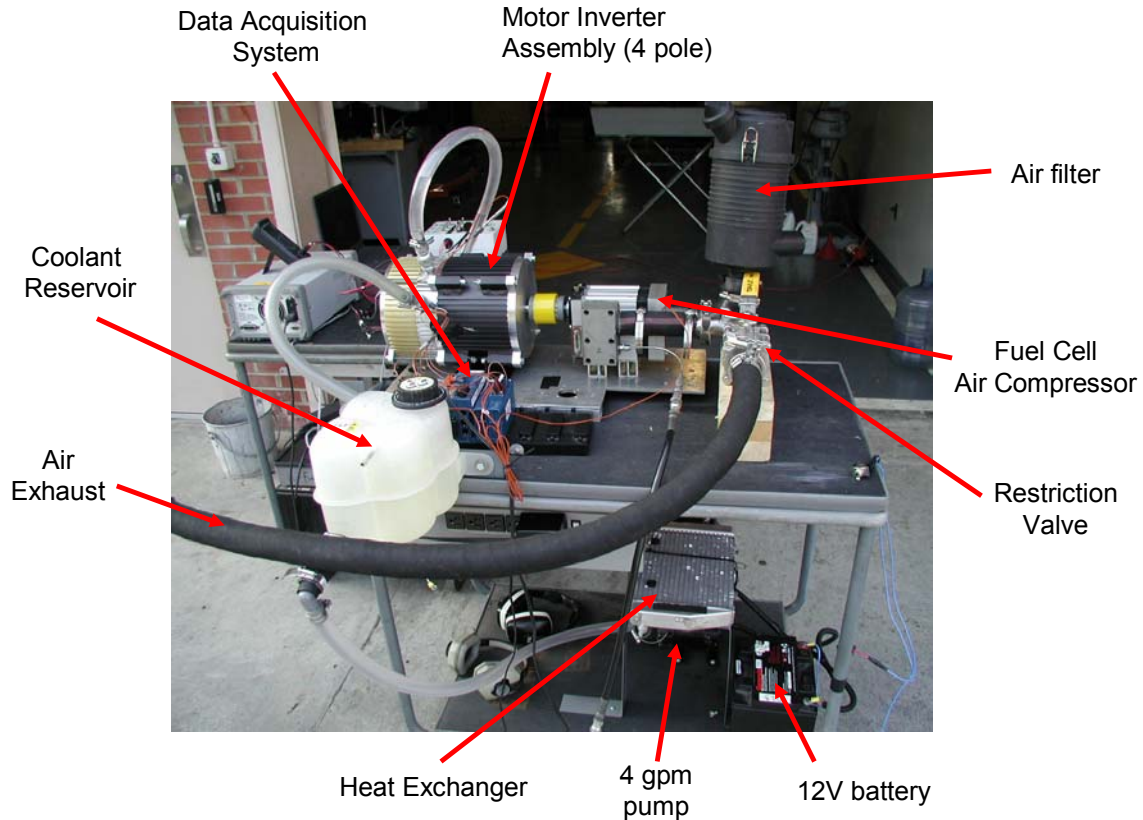


Figure 32: Air compressor motor coupling and coolant system

Before each test the compressor is heated with a heat gun to heat the lubrication fluid and to expand the screws. The coolant system is run before the test until all temperatures reach a steady state.

The compressor is run up to a set speed with a determined load. The load is established through the air pressure by valve adjustment. The speed is run constant and components heat up to operating temperature while the monitoring system logs all the data. The test is terminated when temperatures reach steady state or a component reaches a critical temperature.

7.2 Experimental results

The compressor speed was 10000 rpm and the throttle was closed to the 10 psi setting established in earlier test run. Figure 33 shows the temperature measurements for the test. The highest temperature is the air temperature at the outlet of the compressor. This information along with air pressure and the compressor speed allows establishing the power level the motor ran at. The full test shows that the limiting factor will be the winding temperature. Relative to the coolant temperature the IGBT experiences a temperature rise of only 4 deg C.

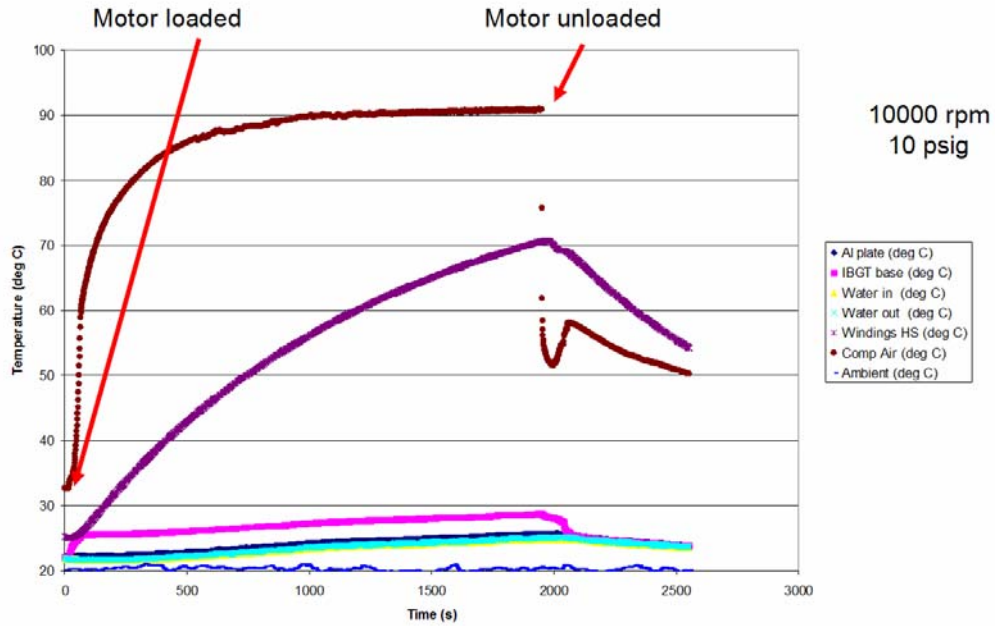


Figure 33: Complete motor inverter unit test results (10000 rpm & 10 psi)

The results also show the thermal capacity of the coolant system. The coolant temperature keeps rising slowly. The radiator can not reject all the heat from the coolant to the ambient temperature at this low of a coolant temperature. Again this coolant system does not have any ram air but only a fan pushing air through it. The system is close to its maximum power point.

7.3 Comparison to model

Figure 34 shows the model results. The motor model is validated by this test. The windings get the hottest. The temperature probe is on the motor side. The model is still a bit on the conservative side and predicts a temperature which is 2 or 3 deg C above the measured data. Notice the center is a little warmer, which can be explained by larger heat inputs. The stator end closer to the cold plate is a few deg colder due to the proximity of the cold plate.

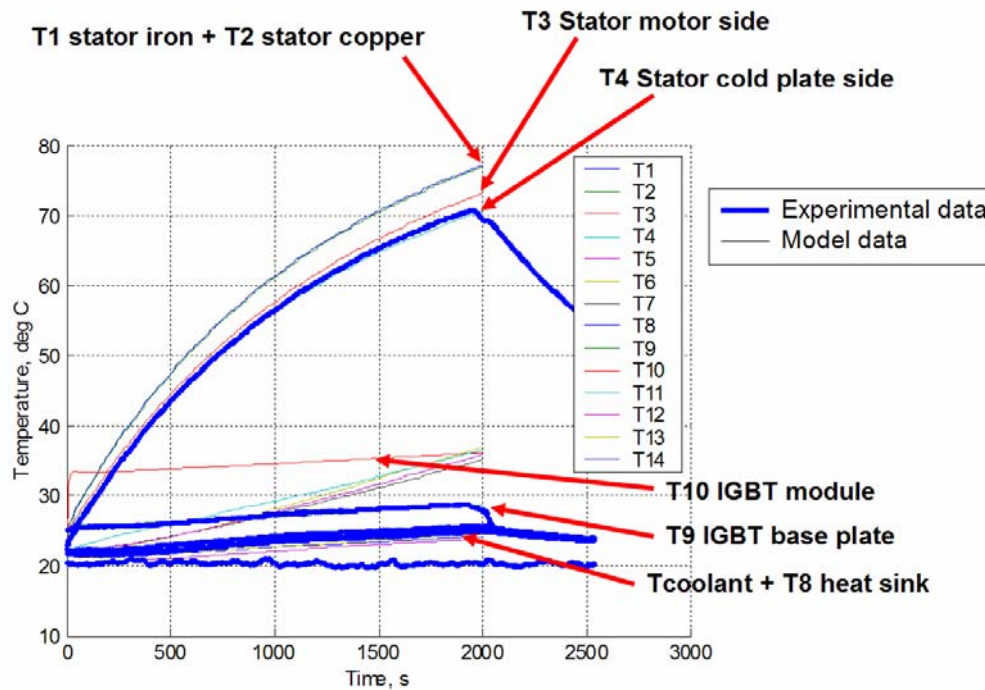


Figure 34: Full test model results with empirical data

The thermal resistances between the motor components and the cold plate are relatively high. Currently the team is investigating the ways of increasing the heat transfer between the motor components and cold plate. A solution is to integrate thermally conductive material between the casing and the windings. That will help to dissipate the heat to the case.

The IGBT temperature is well below its 125 deg C limiting temperature. The thermal resistance is based on the spec sheet shown in Table 3. The base plate temperature corresponds to the model predictions. The coolant capacitance and thermal system model overlay pretty well with the empirical data.

7.4 Conclusion and model adjustments

This test and other full motor inverter tests allowed adjustment of a few contact resistances. On this test stand thermal capacity and other parameters were known and the model could be tuned to model the data.

The full test validates the model. The highest temperatures are expected in the motor and the inverter temperatures reach steady temperatures pretty quickly.

8 Validation and review of the model

8.1 Steady state

The steady state portion of the model refers to the final temperatures once they have reached steady values. On the inverter components and the heat sink the model does reach temperatures which are within 5 to 10% of the empirical data. The model over estimates the temperatures slightly, due to the conservative nature of some of the resistances. So the model predicts the worst case scenario.

8.2 Transients

The transient components of the model are validated by how well the temperatures follow the curves of the empirical data. The model presents good transient response. All the model temperatures follow the empirical curves extremely well. The transient response of the individual lumped mass affects the temperatures of the other lumped mass. So if the transient response of the system is good, the individual transient behaviors are validated, as it is the case with this model.

9 Transient limitation of the unit and overload capabilities

9.1 Physical limiting factors

As stated earlier in Table 5 the limiting factors are the IGBT and the plastic slot liners in the stator windings.

Table 5: Major thermal limiting factor of the inverter and motor

	Limiting temperature	Comment
IGBT	125 deg C	Exceeding temperature results in power loss or damage to the device
Copper Stator windings	160 deg C	Exceeding temperature results in damage of the plastic slot liners

9.2 Maximum power condition

The fuel cell system maximum continuous power output requires the air compressor to provide its maximum continuous power as well. In the vehicle, the system can be exposed to high ambient temperatures especially in a closed engine bay. The worst case estimated is 60 deg C, thus the model is run with ambient conditions and all lumped masses at 60 deg C at the start.

Figure 35 presents the results of the simulation. After an hour of run time none of the components have reached any critical temperatures. Although some parts have not reached a steady state, there is no danger of harming anything. Also it is rather rare that automotive systems operate at maximum power continuously for an hour.

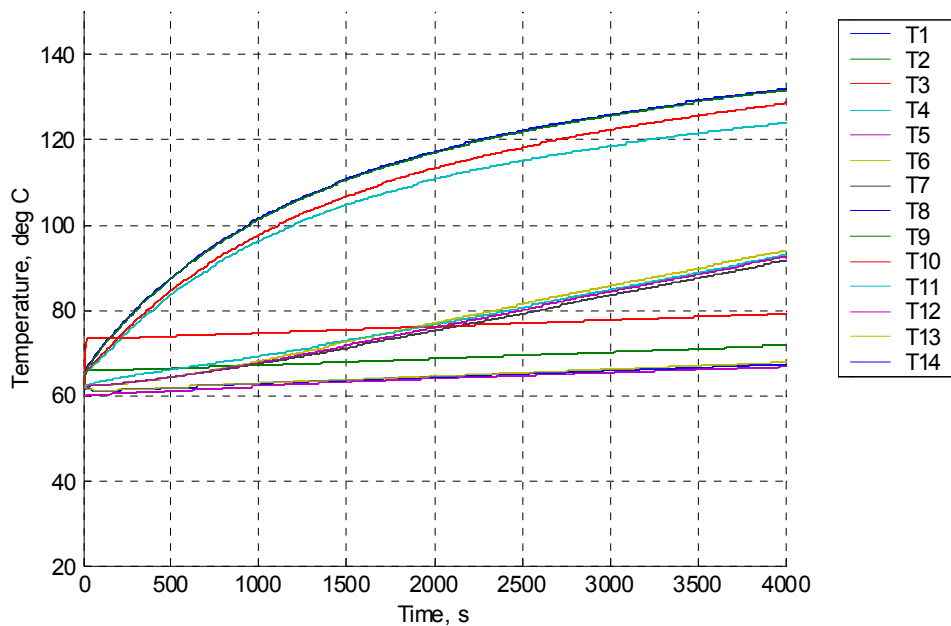


Figure 35: Maximum continuous power run simulation

9.3 Double current condition

The double current situation does refer to a case where the power is doubled. This could occur for a short period of time if the fuel cell system needs to provide more power than its continuous maximum power. The doubled power situation is also in effect when the motor has to spin the compressor up against the full load to full speed.

The graph on the left side in Figure 36 illustrates the simulation results. The thermal limit on the plastic liners in the stator is reached. The IGBT temperature is not a problem. Starting out at 60 deg C the system can run double power for 8 minutes. The IGBT is still below its maximum temperature limit.

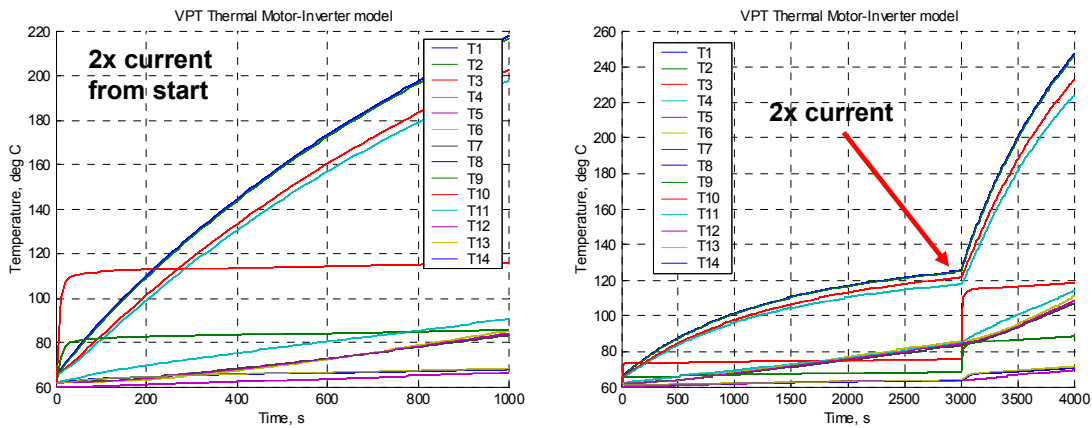


Figure 36: Double current simulation

The graph on the right side in Figure 36 simulates a normal operating condition and once all mass have reached operating temperatures, the double current condition is applied. In these more realistic conditions the system reaches thermal overload in 4 minutes.

10 System strategies to improve the thermal limits

10.1 Active flow control

One solution to influence or delay the thermal limits is to use a variable speed pump. In this section the model is used to simulate the maximum power situation with a flow rate of 6 gpm, thus double the flow rates used. Figure 37 represents the simulation results.

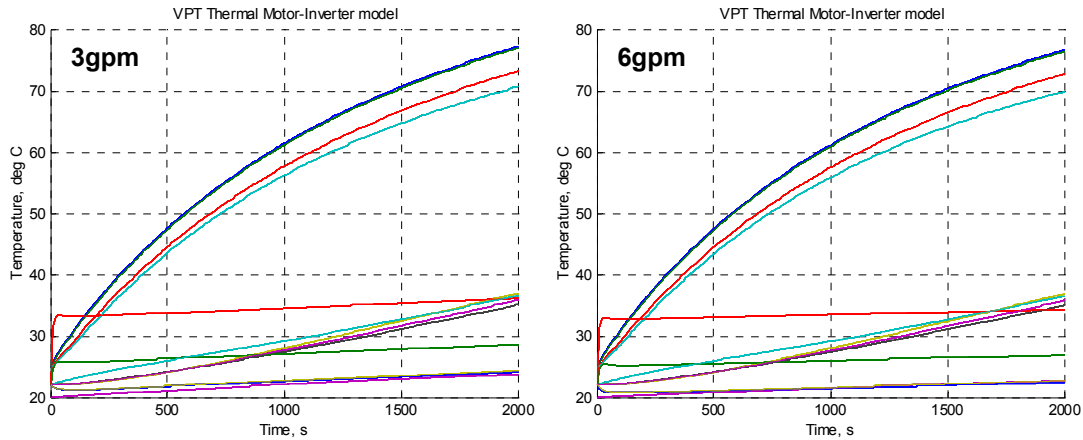


Figure 37: Flow influence over the system

The flow control has an impact on the inverter components. The IGBT and its base plate are a few degrees cooler. The large contact resistances between the motor and the heat sink result in an extremely low impact on the motor temperatures. So an active flow control would not be effective.

10.2 Capacity of the thermal reservoir

The other approach is to increase the thermal capacity of the coolant system. The high thermal capacity adds a larger energy absorption buffer to the system. The temperatures of the coolant will be slower to respond, thus providing a buffer to absorb transient energy and increasing the time to reach limiting temperatures. In the next set the thermal capacity of the coolant system is doubled. Figure 38 represents the simulation results.

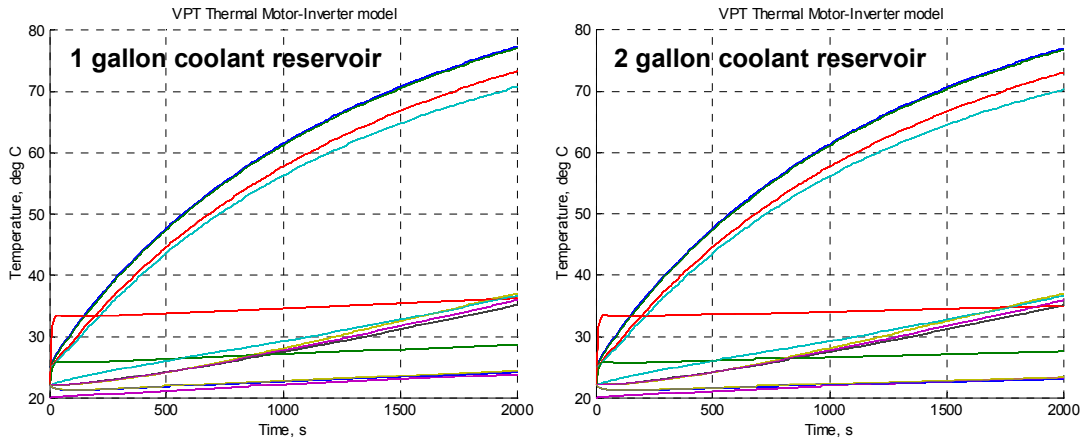


Figure 38: Thermal capacity influence on the system

Again the contact resistance is so large the effect on the motor is minor. The large contact resistance is due to the tie rod system that holds the unit together. The heat sink machined surface is compressed against the machined aluminum surface of the motor. Even with the use of thermal grease the surface irregularities are too large, resulting in a large contact resistance. In a real implementation this means doubling the size of the coolant reservoir which is challenging with the complex packaging of hybrid fuel cell vehicles.

11 Conclusion

A 12 kW compact high speed AC induction inverter motor unit was developed and the thermal design is effective. The cooling system for the high speed AC induction motor and inverter unit enables operation of the unit at the continuous power rating of 12 kW.

A heat sink was designed for this unique assembly. The cold chamber design was developed based on a model and tested on a prototype. The empirical data allowed tuning of the model. The model allowed to reach an optimal design.

A lumped capacitance finite difference model was developed to simulate the entire motor inverter assembly. The model is calibrated and validated in several steps. The inverter side was tested separately from the motor and the model was validated using test data. The entire unit was tested with an actual fuel cell compressor. Again the model was calibrated and validated with test data. The model is presented in Figure 22.

Using the model, the overload conditions were tested. The limiting thermal factor is the copper winding temperature, which can damage the plastic slot liners. The double current test was simulated and operating temperatures of the system exceeded thermal limits within 4 minutes. Next, possible flow changes and changes in thermal capacity of the system were evaluated. A result of that simulation is that the thermal path between the motor and the heat sink needs to be improved before any strategy can affect the motor side.

I would recommend integrating the motor casing and end plate to the heat sink, rather than building it in sections, thus reducing the thermal contact resistances. Also heat transfer between the copper winding ends in the stator could be coated in material that would bond to the case, thus increasing the heat transfer from the windings to the case.

References

1. James Larminie, Andrews Dicks, Fuel Cell systems Explained, Wiley, Feb 2000, page 105, figure 4.28 and 4.29
2. Galen W. Kulp, "A comparison of two air compressors for PEM fuel cell systems", Virginia Tech MS thesis, December 2001
3. Paul Turnbull, John Kuo, Roy Schultz, Bruce Turner, Thermal Analysis of an Electric Machine for a Hybrid Vehicle, Visteon Corporation, 04ANNUAL-131, 2003
4. Semikrom SKM 100 GD 063 DL,
www.semikron.com/skcweb/e/products/igbte.html
5. Siemens Power Inverter Installation Manual, Copyright © 2000-2004, rev 3.00 Feb 11 '2004
6. Siemens Power Inverters, Installation manual, Metric Mind Engineering, Rev 3.00w, Feb 2004
7. Frank P. Incropera, David P. DeWitt, Fundamentals of Heat and Mass Transfer, 4th ed, Wiley, 1996, p 435,
8. Thermodynamics, An Engineering Approach, Yunus Cengel and Michael Boles, McGraw Hill, 3rd ed, 1998

Appendix 1: Symbol reference guide

A	amperes
A	area
AC	alternating current
Ah	amp hours
ATV	all terrain vehicle
CPES	center for power electronic system
d	diameter
DC	direct current
deg C	degree Celsius
DOE	Department of Energy
EMPCON	Embedded Power Control
gpm	gallon per minute
I	current
IGBT	insulated gate bipolar transistors
kg	kilograms
kW	kilowatts
m	meter
P	power
psi	pounds per square inch
PWM	pulse width modulation
rpm	revolution per minute
s	seconds
V	Voltage
VPT	Virginia Power Technologies
W	watts

Appendix 2: Convection heat transfer details

The convection is modeled using a constant surface temperature energy conservation equation. The basic physical problem is defined in Figure A 1.

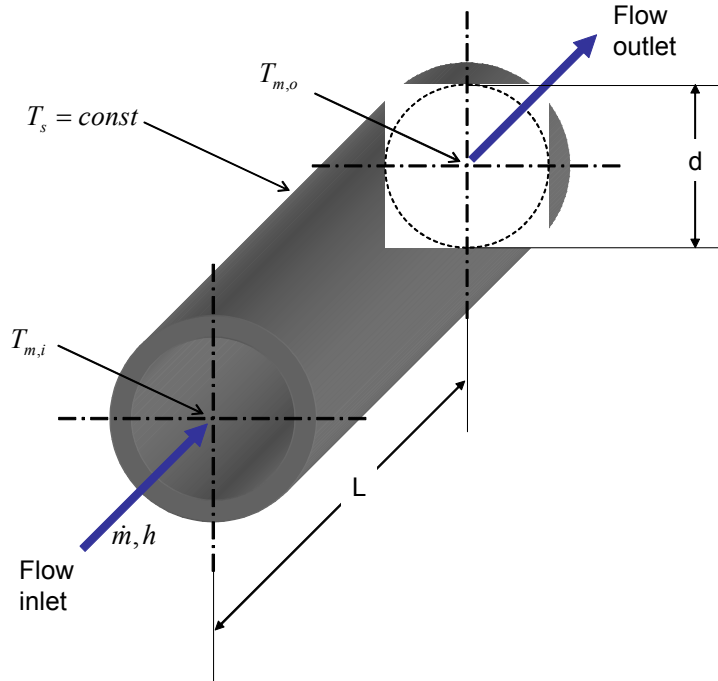


Figure A 1: Illustration of the pipe convection heat transfer

From conservation of the energy, Incropera and DeWitt derive the convection heat transfer for constant surface temperature as shown in Equation A 1.

$$q_{conv} = hA_s \Delta T_{lm} \quad \text{Equation A 1}$$

The area of heat transfer is the surface area of the inner of the pipe, which is the perimeter of the pipe times the length of the pipe. Equation A 2 allows to compute the heat transfer surface.

$$A_s = (\pi d)L \quad \text{Equation A 2}$$

This equation uses the log mean temperature difference as defined in Equation A 3

$$\Delta T_{lm} = \frac{(T_s - T_{m,o}) - (T_s - T_{m,i})}{\log\left(\frac{(T_s - T_{m,o})}{(T_s - T_{m,i})}\right)} \quad \text{Equation A 3}$$

To compute the log mean temperature difference the flow outlet temperature is required. It can be approximated by Equation A 4.

$$T_{m,o} = T_s - (T_s - T_{m,i}) e^{\frac{-hA_s}{\dot{m}c_p}} \quad \text{Equation A 4}$$

The heat transfer coefficient is specified by equation Equation A 5.

$$h = \frac{kNu}{d} \quad \text{Equation A 5}$$

The Nussel number is a dimensionless entity. It can be computed but its expression varies based on the type flow encountered. The turbulent flow increases the heat transfer. Initial calculations show that with a 3 gpm the flow is turbulent expect at really low speed. The program does check for turbulent flow and if this is not the case displays a warning.

For the turbulent case the Nussel number is defined by Equation A 6.

$$Nu = 0.023 Re^{4/5} Pr^n$$

where, $n = 0.4$ for $T_s > T_m$ **Equation A 6**

The Renolds number is defined in Equation A 7.

$$Re = \frac{\rho \dot{m}}{\mu} \quad \text{Equation A 7}$$

The Prandtl for coolant comes from the thermal tables. According to Cengel and Boles (*Cenge,l 1998*) the Prandel number for liquid water at 60 deg C is 2.88 and does not vary much over the temperature range of interest.

$$Pr = 2.88 \quad \text{Equation A 8}$$

Matlab code for the initial calculations

```
This is the file: "pipe_2d.m"
function out=pipe_2d(d,l,gpm)

Ts=70;
Tmi=50;
Tmo=60;

l=l*0.0254;      %m length of the tube
d=d*0.0254;     %m

ro=1000;        %kg/m^3
mu=1.12e-3;    %N.2/m^2
```

```

A=pi/4*d^2;      %m^2
As=pi*d*l;      %m^2

%gpm=3;          %gallon per min
flow=gpm*0.003785/60; %m^3/s
v=flow/A;       %m/s

mdot=flow*ro;

re=ro*d*v/mu;    %dimensionless
Pr=2.88;        %dimensionless @60C Prg=0.960 or Prf=2.88
n=0.4;          %Ts>Tm
Nu=0.023*re^(4/5)*Pr^n;

if re < 2100,
    'none turbulent'
end

cp=4.186*10^3;  %Cpf of water at 335 K
k=656*10^-3;   %Thermal conductivity of water kf=656*10^-3 or kg=22*10^-3

h=Nu*k/d;

Tmo=Ts-(Ts-Tmi)*exp(-h*As/(mdot*cp));
dtm=((Ts-Tmo)-(Ts-Tmi))/(log((Ts-Tmo)/(Ts-Tmi)));
q=h*As*(dtm);

q=mdot*cp*(Tmo-Tmi);

out=[q,Tmo];

```

This is the file: "plotpipe.m"

```

close all
clear all
clc

d=1/2;

for i=1:20
    l(i)=i/1;
    for j=1:10
        gpm(j)=j/1;
        transfer=pipe_2d(d,l(i),gpm(j));
        pipeheat(i,j)=transfer(1);
        pipetemp(i,j)=transfer(2);
    end
end

figure
surf(pipeheat)
tmp=size(pipeheat);
limit(tmp(1),tmp(2))=0;
limit(:,:)=1000;
hold on
surf(limit)
xlabel('flow, gpm')
ylabel('length, in')
zlabel('Heat disipation, W')
title('Heat dissipation vs flow and length. 1-D Steady State model (Pipe 1/2in diameter)')

```

```
figure
surf(pipetemp)
xlabel('flow, gpm')
ylabel('length, in')
zlabel('Outlet temperature, deg C')
title('Outlet temperature vs flow and length. 1-D Steady State model (Pipe
1/2in diameter)')
```

Appendix 3: All the thermal resistances defined

Thermal resistance

R1i4: Stator iron \Leftrightarrow Case

Conduction

$$R1i4 = \frac{dr1i}{k_{steel} \cdot a1i4} + \frac{dr4}{kal \cdot a1i4}$$

R1i1c: Stator iron \Leftrightarrow Stator copper

Conduction

$$R1c1i = ?$$

R1i10: Stator iron \Leftrightarrow Rotor iron

Conduction, convection, radiation

$$R1i10 = \frac{dr1i}{k_{steel} \cdot a1i10} + \frac{1}{h1i10 \cdot a1i10} + \frac{1}{sig1i10 \cdot emis \cdot (T10 + T1i)(T10^2 + T1i^2)} \cdot a1i10 + \frac{dr10}{k_{rotor} \cdot a1i10}$$

R1c2: Stator copper \Leftrightarrow Stator (motor side)

Conduction

$$R1c2 = \frac{dz1c}{k_{copper} \cdot a1c2} + \frac{dz2}{k_{copper} \cdot a1c2}$$

R1c3: Stator copper \Leftrightarrow Stator (cold plate)

Conduction

$$R1c3 = R1c2$$

R24: Stator (motor side) \Leftrightarrow Case

Conduction, convection, radiation

$$R24 = \frac{dr2}{k_{copper} \cdot a24} + \frac{1}{h24 \cdot a24} + \frac{1}{sig24 \cdot emis \cdot (T4 + T2)(T4^2 + T2^2)} \cdot a24 + \frac{dr4}{kal \cdot a24}$$

R25: Stator (motor side) \Leftrightarrow Case

Conduction, convection, radiation

$$R25 = \frac{dz2}{k_{copper} \cdot a25} + \frac{1}{h25 \cdot a25} + \frac{1}{sig25 \cdot emis \cdot (T5 + T2)(T5^2 + T2^2)} \cdot a25 + \frac{dz5}{kal \cdot a25}$$

R34: Stator (cold plate side) \Leftrightarrow Case

Conduction, convection, radiation

$$R34 = R24$$

R313: Stator (motor side) \Leftrightarrow End plate (cold plate side)

Conduction, convection, radiation

$$R_{313} = R_{25}$$

R413: End plate (cold plate side) ⇔ Case
Conduction

$$R_{413} = \frac{dz_{13}}{k_{al} \cdot a_{413}} + \frac{dz_4}{k_{al} \cdot a_{413}}$$

R45: End plate (motor side) ⇔ Case
Conduction

$$R_{45} = R_{413}$$

R4amb: Case ⇔ Atmosphere
Conduction, convection, radiation

$$R_{4amb} = \frac{dr_4}{k_{al} \cdot a_{4amb}} + \frac{1}{h_{4amb} \cdot a_{4amb}} + \frac{1}{\text{sig}_{4amb} \cdot \text{emis} \cdot (T_{amb} + T_4)(T_{amb}^2 + T_4^2)} \cdot a_{4amb}$$

R56: End plate (motor side) ⇔ Shaft
Conduction, convection, radiation

$$R_{56} = \frac{dr_5}{k_{al} \cdot a_{56}} + \frac{1}{h_{56} \cdot a_{56}} + \frac{1}{\text{sig}_{56} \cdot \text{emis} \cdot (T_5 + T_6)(T_5^2 + T_6^2)} \cdot a_{56} + \frac{dr_6}{k_{steel} \cdot a_{56}}$$

R510: End plate (motor side) ⇔ Rotor
Conduction, convection, radiation

$$R_{510} = \frac{dr_5}{k_{al} \cdot a_{510}} + \frac{1}{h_{510} \cdot a_{510}} + \frac{1}{\text{sig}_{510} \cdot \text{emis} \cdot (T_5 + T_{10})(T_5^2 + T_{10}^2)} \cdot a_{510} + \frac{dr_{10}}{k_{rotor} \cdot a_{510}}$$

R511: End plate (motor side) ⇔ Bearing
Conduction

$$R_{511} = \frac{dz_5}{k_{al} \cdot a_{511}} + \frac{dz_{11}}{k_{steel} \cdot a_{511}}$$

R610: Shaft ⇔ Rotor
Conduction

$$R_{610} = \frac{dz_6}{k_{steel} \cdot a_{610}} + \frac{dz_{10}}{k_{rotor} \cdot a_{610}}$$

R611: Shaft ⇔ Bearing (air compressor side)
Conduction

$$R_{611} = \frac{dz_6}{k_{steel} \cdot a_{611}} + \frac{dz_{11}}{k_{steel} \cdot a_{611}}$$

R612: Shaft ⇔ Bearing (cold plate side)
Conduction

$$R_{612} = R_{611}$$

R1011: Bearing (motor side) \Leftrightarrow Rotor iron
Conduction

$$R1011 = \frac{dz10}{k_{rotor} \cdot a1011} + \frac{dz11}{k_{steel} \cdot a10a11}$$

R1012: Rotor iron \Leftrightarrow Bearing (cold plate)
Conduction

$$R1012 = R1011$$

R1013: End plate (cold plate side) \Leftrightarrow Rotor
Conduction, convection, radiation

$$R1013 = R510$$

R1213: Bearing (cold plate) \Leftrightarrow End plate (cold plate side)
Conduction

$$R1213 = \frac{dz12}{k_{steel} \cdot a1213} + \frac{dz13}{k_{al} \cdot a1213}$$

R713: End plate (cold plate side) \Leftrightarrow Cold plate
Conduction

$$R713 = \frac{dz7}{k_{iron} \cdot a713} + \frac{dz13}{k_{iron} \cdot a713}$$

R78: Cold plate \Leftrightarrow Mounting plate
Conduction

$$R78 = \frac{dz7}{k_{iron} \cdot a78} + \frac{dz8}{k_{iron} \cdot a78} + R89c + R89s$$

$R89c$ is the spreading resistance

$R89s$ is the contact resistance

R78: Mounting plate \Leftrightarrow IGBT's
Conduction

$$R78 = R_{spec}$$

Appendix 4: The code to the thermal model

“Main.m”

```
% VPT Thermal Motor Model
% Summer 2003 Last version
% Henning Lohse-Busch (hen@vt.edu)

%Clean the workspace
clear all
close all
clc

%_____INPUTS_____
%Time parameters
dt=.005;
tmax=5000;

%Sampling period for temperatures
Psample=10;      %WARNING it needs to a multiple of the dt

%Initial Conditions
Tini=initialtemperatures;

Tini(1)=25;
Tini(2)=25;
Tini(3)=25;
Tini(4)=25;
Tini(5)=20;

%Physical properties
out=setup(Tini);
R=out(:,1:15);
C=out(:,16);

%Heaksink parameters
Tcoolantini=20.01;
Fcoolant=5;      %coolant flow in gpm

%Losses in the motor inverter
speed=10000;
qgen=losses(speed);

%Initializing error codes and verifications of input
flag=mechanicssetup(dt,Psample);

%_____COMPUTATIONS_____
tic
FDout=finitedifference(dt,tmax,Psample,Tini,C,R,qgen,Tcoolantini,Fcoolant);
toc

%Unpakcing FDout
time=FDout(:,1);
T=FDout(:,2:16);
qgen=FDout(:,17:30);

%_____Energy balance_____
for i=1:length(T(:,1))
    Energycheck(dt,i,T(i,:),C,qgen(i,:))
end

%_____DISPLAY_____
```

```
error_message(flag)
graph(FDout)
```

```
%
% _____ IMPORT DATA AND DISPLAY _____ %
a=importdata(['fulltest.txt']);
dataname=a.colheaders;
data = a.data;
data(:,1)=data(:,1)-16;
figure(100)
plot(data(:,1),data(:,2),'.')
hold on
plot(data(:,1),data(:,3),'.')
plot(data(:,1),data(:,4),'.')
plot(data(:,1),data(:,5),'.')
plot(data(:,1),data(:,6),'.')
plot(data(:,1),data(:,8),'.')
plot(data(:,1),data(:,9),'.')
title('VPT Motor Inverter Testing')
grid on
```

“initialtemperatures.m”

```
function Tini=initialtemperatures
% This function initializes the temperatures for all the lumped mass in the
% network. These temperatures can be manually set in this file.
```

```
Tiniall=20;
```

```
Tini(1)=Tiniall;    %(deg C) Temperature of Center of Stator copper
Tini(2)=Tiniall;    %(deg C) Temperature of Center of Stator iron
Tini(3)=Tiniall;    %(deg C) Temperature of Stator (motor side)
Tini(4)=Tiniall;    %(deg C) Temperature of Stator (Heat sink side)
Tini(5)=Tiniall;    %(deg C) Temperature of Case
Tini(6)=Tiniall;    %(deg C) Temperature of End plate motor side
Tini(7)=Tiniall;    %(deg C) Temperature of Shaft
Tini(8)=Tiniall;    %(deg C) Temperature of Heat sink
Tini(9)=Tiniall;    %(deg C) Temperature of Mounting plate
Tini(10)=Tiniall;   %(deg C) Temperature of IGBT's
Tini(11)=Tiniall;   %(deg C) Temperature of Rotor
Tini(12)=Tiniall;   %(deg C) Temperature of Bearing (motor side)
Tini(13)=Tiniall;   %(deg C) Temperature of Bearing (heat sink side)
Tini(14)=Tiniall;   %(deg C) Temperature of End plate heat sink side
Tini(14)=Tiniall;   %(deg C) Temperature of End plate heat sink side
Tini(15)=Tiniall;   %(deg C) Temperature of End plate heat sink side
```

“setup.m”

```
function out=setup(T)
% This function defines the thermal resistances and thermal capacities
% based on material properties, dimensions, and arrangements
```

```
%
% INPUT Variables
% Tini is an array containing the initial temperatures
```

```
%
%OUTPUT
% out=[R,C]
% R matrix of thermal resistances
% C thermal capacities%
%
```

```
%Defining thermal conductivities
```



```

kiron=69.5;      % (W/m.K) Thermal conductivity of iron 400K
ksteel=56.7;    % (W/m.K) Thermal conductivity of steel 400K
kal=174;        % (W/m.K) Thermal conductivity of aluminum cast alloyt 195 400K
kcopper=393;   % (W/m.K) Thermal conductivity of copper pure 400K
kno=0;         % air no cond

```

```

%Setup of the matrix of thermal resistances
R=zeros(length(T));
emis=1;

```

```

%Estblsihing the ground dimensions

```

```

r(1)=0.75/2*2.54/100;
r(2)=1.6/2*2.54/100;
r(3)=1*2.54/100;
r(4)=1.1*2.54/100;
r(5)=3.71*2.54/100;
r(6)=3.9*2.54/100;
r(7)=5*2.54/100;
r(8)=5.7*2.54/100;
r(9)=6.8*2.54/100;
r(10)=7.5*2.54/100;
r(11)=8*2.54/100;
z(1)=1.47*2.54/100;
z(2)=1.84*2.54/100;
z(3)=2.29*2.54/100;
z(4)=2.74*2.54/100;
z(5)=3.54*2.54/100;
z(6)=4.09*2.54/100;
z(7)=7.59*2.54/100;
z(8)=8.14*2.54/100;
z(9)=8.94*2.54/100;
z(10)=9.34*2.54/100;
z(11)=9.84*2.54/100;
z(12)=10.21*2.54/100;
z(13)=11.42*2.54/100;
z(14)=11.57*2.54/100;

```

```

%Computation of the non-zero thermal resistances

```

```

R(1,2)=1;

```

```

dr1=(r(10)-r(7))/2;
A15=2*r(10)*pi*(z(7)-z(6));
h15=0;
sig15=0;
dr5=(r(11)-r(10))/2;
R(1,5)=resistance(dr1,kiron,A15,h15,sig15,emis,T(1),T(5),dr5,kal);

```

```

A111=2*r(6)*pi*z(7)-z(8);
h111=50;
sig111=1;
dr11=r(6)/2;
R(1,11)=resistance(dr1,kiron,A111,h111,sig111,emis,T(1),T(11),dr11,ksteel);

```

```

dz2=(z(7)-z(6))/2;
A23=pi*(r(9))^2-pi*(r(8))^2;
h23=0;
sig23=0;
dz3=(z(6)-z(3))/2;
R(2,3)=resistance(dz2,kcopper,A23,h23,sig23,emis,T(2),T(3),dz3,kcopper);

```

```

A24=A23;
h24=0;

```

```

sig24=0;
dz4=dz3;
R(2,4)=resistance(dz2, kcopper, A24, h24, sig24, emis, T(2), T(4), dz4, kcopper);

dr3=(r(9)-r(8))/2;
A35=2*pi*r(10)-2*pi*r(9);
h35=50;
sig35=1;
dr5=(r(11)-r(10))/2;
R(3,5)=resistance(dr3, kcopper, A35, h35, sig35, emis, T(3), T(5), dr5, kal);

dz3=(z(6)-z(3))/2;
A36=pi*(r(9))^2-pi*(r(8))^2;
h36=50;
sig36=1;
dz6=(z(2)-z(1))/1;
R(3,6)=resistance(dz3, kcopper, A36, h36, sig36, emis, T(3), T(6), dz6, kal);

dr4=dr3;
A45=A35;
h45=h35;
sig45=sig35;
R(4,5)=resistance(dr4, kcopper, A45, h45, sig45, emis, T(4), T(5), dr5, kal);

A414=A36;
h414=h36;
sig414=sig36;
dz14=dz6;
R(4,14)=resistance(dz4, kcopper, A414, h414, sig414, emis, T(4), T(14), dz14, kal);

dz5=(z(11)-z(2))/2;
A56=pi*(r(11))^2-pi*(r(10))^2;
h56=0;
sig56=0;
dz6=(z(2)-z(1))/2;
R(5,6)=resistance(dz5, kal, A56, h56, sig56, emis, T(5), T(6), dz6, kal);

A514=A56;
h514=h56;
sig514=sig56;
dz14=dz6;
R(5,14)=resistance(dz5, kal, A514, h514, sig514, emis, T(5), T(14), dz14, kal);

A515=2*pi*r(11)*(z(7)-z(6));
h515=50;
sig515=1;
dz15=0;
R(5,15)=resistance(dr5, kal, A515, h515, sig515, emis, T(5), T(15), dz15, kno);

dr6=(r(11)-r(6))/2;
A67=pi*(r(1))^2;
h67=50;
sig67=1;
dr7=r(7)/2;
R(6,7)=resistance(dr6, kal, A67, h67, sig67, emis, T(6), T(7), dr7, ksteel);

A611=pi*(r(6))^2-pi*(r(4))^2;
h611=50;
sig611=1;
dz11=(z(8)-z(5));
R(6,11)=resistance(dz6, kal, A611, h611, sig611, emis, T(6), T(11), dz11, ksteel);

A612=pi*(r(3))^2-pi*(r(1))^2;

```

```

h612=0;
sig612=0;
dz12=(z(4)-z(2))/2;
R(6,12)=resistance(dz6,kal,A612,h612,sig612,emis,T(6),T(12),dz12,ksteel);

A711=2*pi*(r(3))*(z(7)-z(6));
h711=0;
sig711=0;
dr11=(r(6)-r(2))/2;
R(7,11)=resistance(dr7,ksteel,A711,h711,sig711,emis,T(7),T(11),dr11,ksteel);

A712=2*pi*r(2)*(z(3)-z(2));
h712=50;
sig712=1;
dr12=(r(3)-r(1))/2;
R(7,12)=resistance(dr7,ksteel,A711,h711,sig711,emis,T(7),T(11),dr12,ksteel);

A713=A712;
h713=h712;
sig713=sig712;
dr13=dr12;
R(7,13)=resistance(dr7,ksteel,A713,h713,sig713,emis,T(7),T(13),dr13,ksteel);

dz8=0;
A89=1.77*4.133*(0.0254^2);
h89=0;
sig89=0;
dz9=0.157/2;
R(8,9)=resistance(dz8,kal,A89,h89,sig89,emis,T(8),T(9),dz9,kal);

A814=pi*r(11)^2;
h814=0;
sig814=0;
dz14=(z(12)-z(11))/2;
R(8,14)=resistance(dz8,kal,A814,h814,sig814,emis,T(8),T(14),dz14,kal);

R(9,10)=.1;

A1112=pi*r(3)^2-pi*(r(1))^2;
h1112=50;
sig1112=1;
dz12=(z(4)-z(2))/2;
R(11,12)=resistance(dz11,ksteel,A1112,h1112,sig1112,emis,T(11),T(12),dz12,ksteel);

A1113=A1112;
h1113=h1112;
sig1113=sig1112;
dz12=dz12;
R(11,13)=resistance(dz11,ksteel,A1113,h1113,sig1113,emis,T(11),T(13),dz12,ksteel);

A1114=A611;
h1114=h611;
sig1114=sig611;
dz14=dz6;
R(11,14)=resistance(dz11,ksteel,A1113,h1114,sig1114,emis,T(11),T(14),dz14,ksteel);

dz13=dz12;
A1314=A612;
h1314=h612;

```

```

sig1314=sig612;
dz14=dz6;
R(13,14)=resistance(dz13,ksteel,A1314,h1314,sig1314,emis,T(13),T(14),dz14,kal);

%Defining the base specific heats
cpiron=490;      %(J/kg.K) specific heat of iron Incropera table A1
cpsteel=487;    %(J/kg.K) specific heat of steel Incropera table A1
cpal=903;      %(J/kg.K) specific heat of aluminum Incropera table A1
cpcopper=385;  %(J/kg.K) specific heat of copper Incropera table A1

%Applying the cp to the lumped masses
cp(1)=cpsteel;  %(J/kg.K) Specific heat of Stator copper
cp(2)=cpcopper; %(J/kg.K) Specific heat of Center of Stator iron
cp(3)=cpcopper; %(J/kg.K) Specific heat of Stator (motor side)
cp(4)=cpcopper; %(J/kg.K) Specific heat of Stator (Heat sink side)
cp(5)=cpal;    %(J/kg.K) Specific heat of Case
cp(6)=cpal;    %(J/kg.K) Specific heat of End plate motor side
cp(7)=cpsteel; %(J/kg.K) Specific heat of Shaft
cp(8)=cpal;    %(J/kg.K) Specific heat of Heat sink
cp(9)=cpal;    %(J/kg.K) Specific heat of Mounting plate
cp(10)=cpcopper; %(J/kg.K) Specific heat of IGBT's
cp(11)=cpsteel; %(J/kg.K) Specific heat of Rotor
cp(12)=cpsteel; %(J/kg.K) Specific heat of Bearing (motor side)
cp(13)=cpsteel; %(J/kg.K) Specific heat of Bearing (heat sink side)
cp(14)=cpal;   %(J/kg.K) Specific heat of End plate heat sink side

%Defining densities
roiron=7810;    %(kg/m^3) Density Incropera table A1
rocopper=1358; %(kg/m^3) Density Incropera table A1
rosteel=7854;  %(kg/m^3) Density Incropera table A1
roal=2790;     %(kg/m^3) Density Incropera table A1

%Computation of the different lumped masses
m(1)=8.5*0.45359237; %(kg) Mass of Center of Stator copper
m(2)=24.35/3*0.45359237; %(kg) Mass of Center of Stator iron
m(3)=24.35/3*0.45359237; %(kg) Mass of Stator (motor side)
m(4)=24.35/3*0.45359237; %(kg) Mass of Stator (Heat sink side)
m(5)=(pi*r(11)^2-pi*r(10)^2)*(z(11)-z(2))*1.5*roal; %(kg) Mass of Case
m(6)=pi*r(11)^2*(z(2)-z(1))*roal; %(kg) Mass of End
plate motor side
m(7)=(pi*r(3)^2*(z(11)-z(3))+pi*r(1)^2*z(3))*rosteel; %(kg) Mass of Shaft
m(8)=((pi*r(11)^2-pi*r(10)^2)*(z(13)-z(12))+pi*r(11)^2*0.25*2.54/100)*roal;
%(kg) Mass of Heat sink
m(9)=A89*4/1000*rocopper; %(kg) Mass of
Mounting plate
m(10)=0.136; %(kg) Mass of IGBT's
m11al=1.5*0.45359237; %(kg) Mass of Rotor (al)
m11steel=7.7*0.45359237; %(kg) Mass of Rotor (steel)
m(11)=m11al+m11steel; %(kg) Mass of Rotor (steel)
m(12)=50/1000; %(kg) Mass of Bearing (motor side)
m(13)=50/1000; %(kg) Mass of Bearing (heat sink side)
m(14)=pi*r(11)^2*(z(12)-z(11))*roal; %(kg) Mass of End plate heat sink side

%Computation of the thermal capacities
C(1)=m(1)*cp(1); %(J/K) Thermal Capacity of Stator copper
C(2)=m(2)*cp(2); %(J/K) Thermal Capacity of Center of Stator iron
C(3)=m(3)*cp(3); %(J/K) Thermal Capacity of Stator (motor side)
C(4)=m(4)*cp(4); %(J/K) Thermal Capacity of Stator (Heat sink side)
C(5)=m(5)*cp(5); %(J/K) Thermal Capacity of Case
C(6)=m(6)*cp(6); %(J/K) Thermal Capacity of End plate motor side
C(7)=m(7)*cp(7); %(J/K) Thermal Capacity of Shaft
C(8)=m(8)*cp(8); %(J/K) Thermal Capacity of Heat sink
C(9)=m(9)*cp(9); %(J/K) Thermal Capacity of Mounting plate

```

```

C(10)=m(10)*cp(10);      % (J/K) Thermal Capacity of IGBT's
C(11)=m(11)*cp(11);      % (J/K) Thermal Capacity of Rotor
C(12)=m(12)*cp(12);      % (J/K) Thermal Capacity of Bearing (motor side)
C(13)=m(13)*cp(13);      % (J/K) Thermal Capacity of Bearing (heat sink side)
C(14)=m(14)*cp(14);      % (J/K) Thermal Capacity of End plate heat sink side
C(15)=10^9;

out=[R,C'];

```

“resistance.m”

```

function R=resistance(da,ka,A,h,sig,emis,Ta,Tb,db,kb)
%
% This function computes the thermal resistance based on the input
% parameters
%
% INPUT Variables
% da is the tickness of the first mass that the heat is conducted through
% ka is the conductance of the first mass
% A is the area though which the conduction and convection occurs
% h is the convective coeficient
% sig is the radiation constant
% emis is the emissivity
% Ta is the temperature of the first lumped mass
% Tb is the temperature of the second lumped mass
% db is the tickness of the second mass that the heat is conducted through
% kb is the conductance of the second mass
%
%OUTPUT
% R (one number) thermal resistance
%
if ka==0,a=0;else,a=da/(ka*A);end
if h==0,b=0;else,b=1/(h*A);end
if sig==0,c=0;else,c=1/(sig*emis*(Ta+Tb)*(Ta^2+Tb^2)*A);end
if kb==0,d=0;else,d=db/(kb*A);end

R=a+b+c+d;

```

“losses.m”

```

function qgen=losses(speed)
% This function looks up the losses in the motor and the power electronics
% in order to assign these to generated heat within the motor.

%Defining losses [column speed,Stator Cu,Rotor Cu,Iron Loss,Stray Loss]
losses=[0      157.1  88.9   0.4    0.0;
1000  157.1  88.2  13.2   3.1;
2000  157.1  87.8  32.7   8.6;
3000  157.1  87.5  56.6  15.6;
4000  157.1  87.3  84.1  23.8;
5000  157.1  87.1  114.7 33.2;
6000  157.1  86.9  148.0 43.4;
7000  157.1  86.7  183.9 54.6;
8000  157.1  86.5  222.1 66.5;
9000  157.1  86.4  262.6 79.2;
10000 157.1  92.0  266.4 98.7;
11000 157.1  99.7  246.1 123.4;
12000 157.1 103.8 235.3 146.4;
13000 157.1 106.3 228.8 169.2;
14000 157.1 108.4 224.4 192.8;

```

```

15000 157.1 110.0 221.5 217.0;
16000 157.1 111.4 219.6 242.0;
17000 157.1 112.5 218.4 267.6;
18000 157.1 113.4 217.7 294.0;
19000 157.1 114.2 217.3 321.0;
20000 157.1 114.8 217.1 348.7;
21000 157.1 115.4 217.2 377.1;];

qgen=losses(speed/1000+1,2:5);

%Potential heat generation within elements
qgen(1)=qgen(4)/2; % (W) heat generated in Center stator
qgen(2)=qgen(1)/3; % (W) heat generated in Center stator copper
qgen(3)=qgen(1)/3; % (W) heat generated in Stator (Motor side)
qgen(4)=qgen(1)/3; % (W) heat generated in Stator (IGBT side)
qgen(5)=0; % (W) heat generated in Case
qgen(6)=0; % (W) heat generated in End plate
qgen(7)=0; % (W) heat generated in Shaft
qgen(8)=0; % (W) heat generated in Cold plate
qgen(9)=0; % (W) heat generated Mounting plate
qgen(10)=150; % (W) heat generated in IGBT base plate
qgen11a=qgen(3); % (W) heat generated in Rotor aluminum
qgen11b=qgen(4)/2; % (W) heat generated in Rotor iron
qgen(11)=qgen11a+qgen11b;
qgen(12)=0; % (W) heat generated in bearing motor side
qgen(13)=0; % (W) heat generated in bearing cold plate
side
qgen(14)=0; % (W) heat generated in end palte cold plate
side
qgen(15)=0;

```

“mechanicssetup.m”

```

function flag=mechanicssetup(dt,Psample)
% This function initializes the error tracking and verifies the input for
% consistency

%Initialize error flag
flag=0;

%Verfication of Psample
if ((Psample/dt)-round(Psample/dt)) ~= 0,
    disp('Psample is not a multiple of dt')
    flag=1;
end

```

“finitedifference.m”

```

function
out=finitedifference(dt,tmax,Psample,Tini,C,R,qgenini,Tcoolantini,Fcoolant)
% This function computes the temperatures of a lumped mass in time and
% keeps track of temperature at desired time steps.
%
% INPUT Variables
% dt is the time step
% tmax is the ending time for the computation
% Psample is the sampling period for temperatures
% Tini is the array of temperatures of the lumped masses at the previous time
% C is the array holding the theraml capacities of the lumped masses
% R is the matrix of thermal resistances associated with lumped masses (inc
% cond, conv, rad)
%

```

```

%OUTPUT
%   out = [time,temperatures] of all the lumped masses at sampled time steps
%
%Computation of the number of time steps
numbertimestep=tmax/dt;

%Initializing the temperatures in the loop
Told=Tini;
Tcoolantold=Tcoolantini;

%Sampling setup
sampler=Psample/dt;

%Initial losses
qgen=qgenini;

%Loop computing the lump mass temperatures in time and sampling the
%temperatures to save
sample=1;
h = waitbar(0,'Computing... If too long reconsider Psample');
for i=1:numbertimestep,

    %Heat sink contribution
    heatsinkout=heatsink(Told(8),Tcoolantold,Fcoolant);
    qgen(8)=-heatsinkout(1);
    Tcoolantnew=heatsinkout(2);

    %One time laps computation
    Tnew=lumpedmassloop(dt,Told,C,R,qgen);
    if (i/sampler)-round(i/sampler) <= 10^-5,
        if (i/sampler)-round(i/sampler) >= -10^-5,
            Tsample(sample,:)=Tnew;
            Tcoolantsample(sample)=Tcoolantnew;
            tsample(sample)=i*dt;

            qgensample(sample,:)=qgen;

            sample=sample+1;
        end
    end
    waitbar(i/numbertimestep,h)
    Told=Tnew;
    Tcoolantold=Tcoolantold+(Tcoolantnew-Tcoolantold)/90*dt;

end
close(h)

heatsinkout=heatsink(Told(8),Tcoolantold,Fcoolant);
qgen(8)=-heatsinkout(1);
Tcoolantnew=heatsinkout(2);

%Packaging results to output
time=[0,tsample]';
T=[Tini;Tsample];
qgensample=[qgensample;qgen];
out=[time,T,qgensample];

```

“heatsink.m”

```

% function out=heatsink(Ts,Tcoolant,Fcoolant)

```

```

%
% qgen=-0;
% Tcoolantout=3;
% out=[qgen,Tcoolantout];
%
function out=heatsink(Ts,Tmi,gpm)

dy=1/4*2.54/100;
n=9;
dia_chamber=8*0.0254;
l=linspace(0,dia_chamber,n);
dx=l(2)-l(1);
for i=1:n-1,
    l_computational(i)=l(i)+(l(i+1)-l(i))/2;
    width(i)=sqrt((dia_chamber/2)^2-(l_computational(i)-(dia_chamber/2)).^2);
end

Tm=Tmi;
q=0;
delta_p=0;

for i=1:n-1,
    tmp=pipe_heat(Tm(i),Ts,dx,dy,width(i),gpm);
    dq(i)=tmp(1);
    Tm(i+1)=tmp(2);
    q=q+dq(i);
end
for i=n:2*n-2,
    tmp=pipe_heat(Tm(i),Ts,dx,dy,width((2*n-1)-i),gpm);
    dq(i)=tmp(1);
    Tm(i+1)=tmp(2);
    q=q+dq(i);
end

Tmo=Tm(end);

out=[q,Tmo];

```

“pipe heat.m”

```

%function q=pipe_heato(Tmi,Tmo,Ts,dx,dy,width,gpm)
function out=pipe_heat(Tmi,Ts,dx,dy,width,gpm)

%Water
ro=1000;           %kg/m^3
mu=1.12e-3;       %N.s/m^2
mu=324e-6;        %N.s/m^2 Incropera
Pr=2.88;          %dimensionless @60C Prg=0.960 or Prf =2.88

% %Ethylene Glycol
% ro=1074;         %kg/m^3
% mu=0.278e-2;    %N.s/m^2
% Pr=55;          %dimensionless @60C Prg=0.960 or Prf =2.88

Ac=dy*width;      %m^2
Per=2*(dy+width); %m Perimeter
d_h=4*(Ac)/(Per); %hydraulic diameter Dh=4*Ac/P p 449 Incropera
As=dx*Per;        %m^2

%gpm=3;           %gallon per min

```



```

flow=gpm*0.003785/60;    %m^3/s
v=flow/Ac;              %m/s

mdot=flow*ro;

re=ro*(d_h)*v/mu;       %dimensionless
n=0.4;                  %Ts>Tm
Nu=0.023*re^(4/5)*Pr^n;

% if re < 2100,
%   '-----None turbulent-----'
%   '-----'
%   re
% end

cp=4.186*10^3;          %Cpf of water at 335 K
k=656*10^-3;           %Thermal conductivity of water kf=656*10^-3 or kg=22*10^-3

h=Nu*k/d_h;

Tmo=Ts-(Ts-Tmi)*exp(-h*As/(mdot*cp));
dtm=((Ts-Tmo)-(Ts-Tmi))/(log((Ts-Tmo)/(Ts-Tmi)));
q=h*As*(dtm);

%q=mdot*cp*(Tmo-Tmi);
out=[q,Tmo];

```

“lumpedmassloop.m”

```

function Tnew=lumpedmassloop(dt,Told,C,R,qgen)
% This function computes the temperatures of a lumped mass for a new time
% step.
%
% INPUT Variables
% dt is the time step
% Told is the array of temperatures of the lumped masses at the previous time
% C is the array holding the thermal capacities of the lumped masses
% R is the matrix of thermal resistances associated with lumped masses (inc
%   cond, conv, rad)
%
% OUTPUT
% Tnew temperatures of all the lumped masses the new time step
%
% Loop computing the energy balance for each lumped mass
for ref=1:length(Told),
    Tnew(ref)=explicitenergybalance(ref,dt,Told,C,R,qgen(ref));
end

```

“explicitenergybalance.m”

```

function Tout=explicitenergybalance(ref,dt,Told,C,R,qgen)
% This function computes the temperature of a lumped mass based on the
% temperatures of the other lumped masses at previous time. This is a
% finite difference energy conservation code.
%
% INPUT Variables
% ref is the reference temperature that is being computed
% dt is the time step
% T is the array of temperatures of the lumped masses at the previous time
% C is the array holding the thermal capacities of the lumped masses
% R is the matrix of thermal resistances associated with lumped masses (inc

```

```

%      cond, conv, rad)
%
%OUTPUT
%      Tout (one number) temperature of the "ref" lumped mass at the new time step
%
%Energy tranfers throught the different path
for i=1:length(R(1,:)),
    if R(i,ref)==0;
        Q(i,ref)=0;
    else
        Q(i,ref)=(Told(ref)-Told(i))/R(i,ref);
    end
end

for j=1:length(R(1,:)),
    if R(ref,j)==0;
        Q(ref,j)=0;
    else
        Q(ref,j)=(Told(ref)-Told(j))/R(ref,j);
    end
end

%Net sum of the heat transfers
Qnet=sum(sum(Q))-qgen;

%Energy conservation Est = Qnet
Tout=Told(ref)-(dt/C(ref))*Qnet;

```

“Energycheck.m”

```
function Energycheck(dt,i,T,C,qgen)
```

```

for j=1:length(T)-1,
    E(j)=C(j)*T(j);
end

```

```
E=sum(E)+sum(qgen);
```

```

figure(101)
hold on
plot(i*dt,E,'.')

```

“error message.m”

```
function error_message(flag)
```

```

% This function displays the possible errors that could have occurred during
% the commputations

```

```

if flag==0,
    disp('No errors occurred during the computation')
end

```

```

if flag==1,
    disp('Psample is not a multiple of dt')
end

```

“graph.m”

```

function graph(T)

time=T(:,1);

% lumps=1:(length(T(1,:))-1);
% surf(lumps,time,T(:,2:length(T(1,:)))));
% xlabel('Lump #')
% ylabel('Time, s')
% zlabel('Temperature, deg C')
% title('VPT Thermal Motor-Inverter model')

figure(100),
hold on
for i=1:(length(T(1,:))-1),
plot(time,T(:,2),...
time,T(:,3),...
time,T(:,4),...
time,T(:,5),...
time,T(:,6),...
time,T(:,7),...
time,T(:,8),...
time,T(:,9),...
time,T(:,10),...
time,T(:,11),...
time,T(:,12),...
time,T(:,13),...
time,T(:,14))
end
xlabel('Time, s')
ylabel('Temperature, deg C')
title('VPT Thermal Motor-Inverter model')
legend(...
'T1',...
'T2',...
'T3',...
'T4',...
'T5',...
'T6',...
'T7',...
'T8',...
'T9',...
'T10',...
'T11',...
'T12',...
'T13',...
'T14')

```

Vita

Henning Lohse-Busch hen@vt.edu

Student Address:
606 Preston Ave
Blacksburg, VA 24060, USA
540-231-7457

Permanent Address:
51, route d'Eguisheim
68920, Wettolsheim, France
03-33-89-79-67-69

Objective	Thesis of the Master of Science in Mechanical Engineering
Education	Master of Science, Mechanical Engineering , accepted in PhD program, January 2003 Virginia Polytechnic Institute and State University, (Virginia Tech), Blacksburg, VA, USA "Thermal overload capability of an electric motor and inverter units through modeling" GPA: 3.85/4.0 Bachelor of Science, Mechanical Engineering , Virginia Tech, 2001, GPA 3.83/4.0, " <i>Summa cum Laude</i> " <ul style="list-style-type: none">• Fall 1999, Virginia Polytechnic Institute and State University, Blacksburg, VA, USA• Spring 1998, Euro-American Institute of Technology, Sophia Antipolis, France• Fall 1997, Clarkson University, Potsdam, NY, USA Baccalauréat Scientifique, spécialité Mathématique, option Informatique , Summer 1997, Munster, France
Engineering Experience	Engineer Assistant , Basic research on shockwave medical machinery, Storz Medical, Kreuzlingen, Switzerland, Summer 1998, 4 weeks Hybrid Electric Vehicle Team of Virginia Tech, HEVT , www.hevt.me.vt.edu, www.futuretruck.org, <ul style="list-style-type: none">• FutureTruck 2001, Fuel Cell Hybrid Vehicle Control group leader, Senior Design• FutureTruck 2002, Fuel Cell Hybrid Team leader assistant, Volunteer• FutureTruck 2003, H₂ICE Hybrid Team leader, Volunteer• FutureTruck 2004, H₂ICE Hybrid Team leader, Graduate Teaching Assistant Graduate Research Assistant for Dr. D.J. Nelson, Virginia Tech <ul style="list-style-type: none">• Fall 2001 Fuel Cell modeling funded by National Renewable Energy Laboratory (NREL)• Fall 2002 Cooling of power electronics funded by Virginia Power Technologies (VPT) Graduate Teaching Assistant for Dr. D.J. Nelson, Virginia Tech <ul style="list-style-type: none">• Fall 2003 ME 4015: Engineering Design and Projects (Fall 2003)
Languages	German : first native language; French : second native language; English : fluently spoken and written
Activities	Society of Automotive Engineers (SAE), Secretary 2002/03 National Mechanical Engineering Honor Society, Pi Tau Sigma, Vice President American Society of Mechanical Engineers (ASME), Professional Development Chair 2000/01 Student Engineering Council (SEC), National Engineering Society, Tau Beta Pi Honor Society for International Scholars, Phi Beta Delta
Awards	<ul style="list-style-type: none">• College of Engineering, Deans List, Fall 1999, Spring 2000 and Fall 2000• IR Student Award, Mechanical Engineering, 2001• Pratt Fellowship, Mechanical Engineering, 2001-2002
Skills	Computer Skills : Microsoft Office XP Pro (Word, Excel, PowerPoint, FrontPage, Access), AutoCAD. Programming languages : C++, Fortran, Matlab (inc Simulink) 6.5, LabVIEW 7, HTML and Java Leadership Skills : Extensive leadership experience with student organizations and class projects; Participated in several leadership conferences (SEC Virginia Tech, RSLAS ASME, FutureTruck among others)
Publications	H Lohse-Busch, T Stinchfield, M Mital, A Hines, DJ Nelson, (2003), "Design and implementation of a hybrid electric vehicle powered by a hydrogen engine," Proceedings of the 2003 FutureTruck Challenge, June 1-12, 2003, Ford Romeo Proving Grounds, MI, SAE paper pending, 18 p S Gurski, H Lohse-Busch, G Henshaw, DJ Nelson, (2002), "Design of a zero emission sport utility vehicle," Proceedings of the 2002 FutureTruck Challenge, June 11-21, 2002, Ford Arizona Proving Grounds, AZ, SAE paper 2000-01-1264, 17 p S Gurski, D Evans, D Knox, M Conover, A Harris, H Lohse-Busch, S Kraft, DJ Nelson, (2002), "Design and Development of the 2001 Virginia Tech FutureTruck: A Fuel Cell Hybrid Electric Vehicle," Proceedings of the 2001 FutureTruck Challenge, June 4-13, 2001, Ford Milford Proving Grounds, MI, SAE paper SP-1701, 18 p
References	Dr. D.J. Nelson doug.nelson@vt.edu Director of automotive fuel cell systems